

Wind-driven Rain on Buildings in Metro Vancouver: Parameters for Rain Penetration  
Testing of Window Assemblies

Ronald Krpan

A Thesis

in

The Department

of

Building, Civil, and Environmental Engineering

Presented in Partial Fulfillment of the Requirements  
for the Degree of Master of Applied Science (Building Engineering) at  
Concordia University  
Montreal, Quebec, Canada

9 January 2013

© Ronald Krpan, 2013

**CONCORDIA UNIVERSITY**

**School of Graduate Studies**

This is to certify that the thesis prepared

By: Ronald Krpan

Entitled: Wind-driven Rain on Buildings in Metro Vancouver:  
Parameters for Rain Penetration Testing of Window Assemblies

and submitted in partial fulfillment of the requirement for the degree of

**Master of Applied Science (Building Engineering)**

complies with the regulations of the University and meets the accepted standards with respect to originality and quality.

Signed by the final examining committee:

\_\_\_\_\_  
Dr. Radu Zmeureanu, Chair

\_\_\_\_\_  
Dr. Yong Zeng, Examiner, external to program

\_\_\_\_\_  
Dr. Andreas Athienitis, Examiner

\_\_\_\_\_  
Dr. Paul Fazio, Co-supervisor

\_\_\_\_\_  
Dr. Hua Ge, Co-supervisor

Approved by

\_\_\_\_\_  
Chair of Department or Graduate Program Director

\_\_\_\_\_  
2013

\_\_\_\_\_  
Dean of Faculty

## ABSTRACT

### Wind-driven Rain on Buildings in Metro Vancouver: Parameters for Rain Penetration Testing of Window Assemblies

Ronald Krpan

Laboratory tests conducted on building assemblies to assess their resistance to rain penetration are commonly conducted by exposing the assemblies to air pressure differentials and water sprayed onto the outer surface to simulate wind-driven rain. The two primary test parameters are magnitude of air pressure differential and water spray rate. To assess the appropriateness of current standards for testing window assemblies exposed to real weather conditions in Metro Vancouver's unique temperate rainforest climate, measurements of hourly wind-driven rain observed at building sites in Metro Vancouver are used to compute corresponding test conditions. Analysis of the observed site data leads to an expression for catch ratio as a function of wind speed. To establish a statistical basis for computing test conditions for specific return periods, the site data are linked to 25 years of average hourly historical data collected by Environment Canada from 1981 to 1996 at the Vancouver International Airport. Based on an extreme distribution analysis of wind speed and driving rain intensity, the water spray rate and air pressure differential corresponding to 10- and 20-year return periods are computed and compared to current standards. Results suggest that the standard for the intensity of rain impinged on window surfaces meets or exceeds measured conditions corresponding to a 20-year return period and are adequate for Metro Vancouver's climate.

## ACKNOWLEDGEMENTS

This thesis was supported by financial and in-kind contributions from the British Columbia Institute of Technology (BCIT), the Canada Mortgage and Housing Corporation, the Home-owner Protection Office of BC, and the BC Housing Management Commission. I am indebted to the many faculty and staff at BCIT and Concordia University for their cooperation and support throughout this project. It is a pleasure to thank Mr. Wayne Hand, Associate Dean of the School of Construction and the Environment at BCIT, and the faculty and staff of both the Architectural and Building Engineering Technology program and the Building Science Centre of Excellence. I am especially grateful for the support of the faculty, staff and students in the Department of Building, Civil and Environmental Engineering at Concordia University. I owe my most heartfelt expression of gratitude to my co-supervisors at Concordia University, Dr. Paul Fazio and Dr. Hua Ge, whose direction and guidance made this thesis possible.

## TABLE OF CONTENTS

LIST OF FIGURES .....	VI
LIST OF TABLES .....	XI
CHAPTER 1: INTRODUCTION .....	1
CHAPTER 2: LITERATURE REVIEW .....	3
2.1 Regional weather and climate context .....	3
2.2 Fundamentals of wind and rain .....	10
2.3 Empirical approaches to quantifying wind-driven rain .....	35
2.4 Test standards and parameters for window testing .....	42
2.5 Correlation of test parameters to field wind-driven rain measurements ...	46
2.6 Summary of findings .....	49
CHAPTER 3: METHOD .....	51
3.1 Gathering and analysis of short-term building site data .....	52
3.2 Analysis of historical airport data .....	62
3.3 Calculation of air pressure differential and water spray rate .....	63
CHAPTER 4: ANALYSIS .....	65
4.1 Analysis of short-term building site data .....	65
4.2 Analysis of historical airport data .....	80
4.3 Calculation of test conditions and comparison to published values .....	85
CHAPTER 5: CONCLUSIONS .....	90
5.1 Conclusions .....	90
5.2 Future research .....	91
REFERENCES	93
APPENDIX: BUILDING DETAILS AND SENSOR LOCATIONS .....	98

## LIST OF FIGURES

Figure 1: Schematic diagram showing upward vertical motion and cloud formation associated with converging surface winds and divergence aloft (upper diagram) and diverging surface winds and convergence aloft (lower diagram). Adapted from (Lutgens & Tarbuck, 1989)..... 5

Figure 2: Schematic diagram showing sea/land breezes over Vancouver during the day (A) and at night (B); and valley/mountain winds during the day (C) and at night (D) (Oke & Hay, 1998) ..... 8

Figure 3: Mean annual precipitation (mm) for Metro Vancouver. Source: (Oke & Hay, 1998). ..... 9

Figure 4: Mean annual wind speed and direction for Metro Vancouver. Source: (Oke & Hay, 1998)..... 9

Figure 5: Stream tubes delineated by stream lines showing velocity and transverse area through which conservation of mass and energy apply (Hucheson & Handegord, 1989) ..... 11

Figure 6: Perturbation in otherwise laminar flow showing increased velocity in constrained stream tube..... 12

Figure 7: Sketch depicting the appearance of vortex pairing showing downstream eddies as larger and fewer in number..... 12

Figure 8: Path to Chaos from perturbation (top) to vortex interaction ..... 12

Figure 9: Development of a turbulent boundary layer on a flat plate (Massey, 1979) ..... 14

Figure 10: Air flow patterns around a rectangular building, including a depiction of the frontal vortex and recirculation zones (American Society of Heating, Refrigerating, and Air-Conditioning Engineers, Inc., 2009).....	16
Figure 11: Boundary layer separation, such as at building corners .....	17
Figure 12: Sketch of a shear layer at the end of a plate separating fluids with a velocity difference .....	17
Figure 13: Typical wetting patterns on a high rise building exposed to wind-driven rain over time showing concentrations along the top edge and at the upper corners of the windward wall (Robinson & Baker, 1975).....	18
Figure 14: Local pressure coefficients ( $C_p \times 100$ ) for tall buildings with wind direction at angles of 0, 15, and 30 degrees measured normal to wall surface (American Society of Heating, Refrigerating, and Air-Conditioning Engineers, Inc., 2009) .....	19
Figure 15: Local pressure coefficients for the windward wall of a low-rise building with wind direction normal to surface (left) and at 45 degrees to the normal (American Society of Heating, Refrigerating, and Air-Conditioning Engineers, Inc., 2009) ....	20
Figure 16: The rain intensity vector with its components of horizontal rainfall intensity and driving rain intensity adapted from Blocken and Carmeliet (2004).....	23
Figure 17: The relationship between horizontal rainfall intensity and driving rain intensity under idealized conditions of steady, uniform and horizontal wind and a single raindrop diameter .....	26
Figure 18: Schematic diagram with orthogonally oriented apertures measuring horizontal rain intensity and driving rain intensity that can be used to establish the rain intensity vector.....	29

Figure 19: A plate driving rain gauge with circular collection area and concealed tipping bucket recording mechanism (photograph courtesy of National Research Council Canada) .....	30
Figure 20: Progression of some milestones in early wind-driven rain research .....	36
Figure 21: Test apparatus with movable chamber and window specimen, air and water nozzles, and associated equipment to control air pressure differentials and water spray rate at Cascadia Windows in Langley, BC.....	43
Figure 22: Window test set-up with a device for rapidly changing the air pressure differential to simulate wind gusts (Lacasse, Moore, & Van Den Bossche, n.d.) ....	46
Figure 23: Map showing location of Keefer, Kingsway and Wallace building sites as well as the Vancouver International Airport.....	53
Figure 24: Photographs of the three buildings (from top): Keefer, a high-rise building with roof overhang located east of the downtown core; Kingsway, a high-rise building located inland at an exposed location; and Wallace, a low and wide building located near waterfront .....	55
Figure 25: Diagram of the wind-driven rain gauge showing dimensions of the diamond-shaped collection area and housing unit for the tipping bucket mechanism (Ge & Krpan, 2009) .....	58
Figure 26: Photograph of a prototype of the wind-driven rain gauge deployed on a campus building .....	58
Figure 27: Sequence of photographs showing the characteristic wetting pattern of a wall of a high rise building in Vancouver with south-east exposure.....	59



Figure 28: Three dimensional plots showing variation of catch ratio with wind speed and horizontal rainfall intensity for the top corner of a low-rise building (left) and high-rise building (Blocken, 2004).....	61
Figure 29: Typical scatter plot of measured catch ratio versus wind speed with fitted curve.....	62
Figure 30: Temporal distribution of wind speed measured at the centre of the roof of the building and 10 metres above its surface .....	69
Figure 31: Frequency distribution of wind speed corresponding to 1 m/s bin intervals... 71	
Figure 32: Frequency distribution of wind direction (128-point rose) measured from north at top.....	72
Figure 33: Temporal distribution of horizontal rainfall intensity .....	74
Figure 34: Temporal distribution of wind-driven rain (WDR) intensity for each gauge at each building site for the period of record .....	76
Figure 35: Temporal distribution of catch ratio for each gauge at each building site for the period of record.....	78
Figure 36: Scatter plot of catch ratio as a function of wind speed showing curves fit to measured data for each building site.....	81
Figure 37: Extreme distribution of wind speeds at the Vancouver airport.....	84
Figure 38: Extreme distribution of horizontal rainfall intensity at the Vancouver airport	84
Figure 39: Extreme distribution of driving rain intensity .....	86
Figure 40: Bar chart showing estimated test pressures based on current study alongside published values.....	88

Figure 41: Bar chart showing estimated water spray rates based on current study

alongside published values..... 89

## LIST OF TABLES

Table 1: MANOBS guide for determining the intensity of rain visually without the aid of instrument measurements (Environment Canada, 1997). .....	24
Table 2: Summary of water penetration test standards and parameters.....	44
Table 3: CSA A440 classification of rain penetration resistance .....	45
Table 4: Adhesion water on vertically aligned plates of varying material .....	57
Table 5: Summary description of the three subject buildings including form and overhang geometry, location description, and general arrangement of wind-driven rain gauges .....	60
Table 6: Name and corresponding wall orientation in degrees for each wind-driven rain gauge at each building site .....	66
Table 7: Average hourly and maximum wind speed for each building site .....	68
Table 8: Average and maximum horizontal rainfall intensity for each building site .....	73
Table 9: Average and maximum wind-driven rain intensities (mm/h) for each gauge at each building site .....	73
Table 10: Estimated test pressures based on current study and summary of published values .....	87
Table 11: Estimated water spray rates associated with 10- and 20-year return periods and standard test spray rates .....	89

## CHAPTER 1: INTRODUCTION

The quantity of rain impinging on surfaces of a building and the coincident wind pressure are important considerations in the design of its windows to resist rain penetration. Laboratory tests of window assemblies are commonly conducted by window manufacturers, certification agencies, and research organizations. Builders and consultants also frequently conduct field tests of installed windows. The tests are intended to assess the resistance of assemblies to rain penetration by applying air pressure differentials across the assembly while spraying water at a controlled rate on the outside surface. The resulting combination of air pressure differential and impinging water is intended to simulate wind-driven rain. The air pressure differential and water spray rate are specified in industry standards, such as CSA A440 (Canadian Standards Association, 2000); however, few measurements of actual wind-driven rain on the walls of buildings have been made to verify the standard for particular climates. A CMHC study (RDH Building Engineering, 2002) of codes, standards, testing, and certification related to the water penetration resistance of windows concluded that the testing and rating systems used for windows may not “have any significance with respect to the in-service performance of the installed window.” The objective of this research is to provide information that may help to improve testing methods for windows by providing estimates of wind-driven rain intensities on buildings in Metro Vancouver.

Three building sites in the Metro Vancouver region are fitted with rain gauges and other instrumentation to collect data on wind-driven rain intensities. The building site data are linked to 25 years of wind and rain data from the Vancouver airport to establish an historical context for the new data and to enable statistical estimation of return periods

corresponding to particular test parameters. The results indicate the wind-driven rain conditions that in-situ windows are likely to experience when exposed to real-weather conditions in Metro Vancouver.

The thesis begins with a review of the fundamentals of wind-driven rain beginning with the influence of weather and climate and including measurement and test methods. A description of the experimental method is presented in Chapter 3, including a description of the subject buildings as well as details of instrumentation and data acquisition systems employed for the study. Chapter 4 presents the analysis and results of the wind and rain measurements collected at each building site as well as an extreme distribution analysis of historical airport data, including calculation of corresponding test conditions. The thesis concludes with Chapter 5, which also includes a summary of contributions and suggestions for future research.

## CHAPTER 2: LITERATURE REVIEW

The literature review begins with an overview of the regional weather and climate context for this study. A review of the fundamentals of wind and rain follows and addresses concepts of atmospheric boundary layer, airflow around buildings, specific catch ratio, measurement methods and several other topics. A brief historical survey on developments in empirical approaches to quantify wind-driven rain is provided, including research on the concept of driving rain indices and the codified British Standard for estimating wind-driven rain intensities. The literature review includes a description of the test methods for simulating wind-driven rain and concludes with a summary of findings.

### 2.1 Regional weather and climate context

Vancouver's mid-latitude location on the west coast of a large continent and an adjacent series of mountain ranges paralleling coastal British Columbia combine to help create its unique climate. A significant global source-region for polar maritime air masses lies to the north west of the region and produces persistent low pressure cells that settle off-shore, west of Vancouver. The region is also significantly influenced by the large scale topographical influences of nearby mountain ranges. The resulting mid-winter conditions are cool and humid with characteristic high rainfall. Located at the mouth of a coastal valley, valley redirection and small scale circulations are also significant.

#### 2.1.1 *Orographic effects*

Orographic lifting and redirection are mechanical process whereby a parcel of air carried by wind is deflected as it encounters a change in topography. For example, the vertical compression of a parcel of air as it approaches a mountain range is matched by a

horizontal divergence, producing a mountain ridge<sup>1</sup>, and is followed by a reverse process on the lee side, producing a lee trough (Barry, 1992). Vancouver's weather is influenced by several major topographical features. It is located at the southern boundary of the Coast Mountains, making orographic lifting a significant influence, and at the mouth of the Fraser River Valley where it opens into the Strait of Georgia, the latter having a redirecting influence on circulations (Oke & Hay, 1998).

### 2.1.2 Aleutian lows and Coastal British Columbia

*"With deep low-pressure cells off the coast and high pressure in the provincial interior, sea-level winds generally blow offshore and parallel to the mountains. With such persistent easterly and southeasterly flow, it is hard to imagine that the Coast Region lies within the belt of the prevailing westerlies."* (Heidorn, 2004)

Downward or upward movements of the air over certain regions, referred to as cells, can raise or lower pressures measured at the surface and significantly affect weather in the vicinity of the cell. Regions of upward air movement, referred to as low pressure cells because of the corresponding decrease in atmospheric pressure that can be measured on the surface, are associated with cloudy skies and increased chances of precipitation while regions of downward air movement, referred to conversely as high pressure cells, are typically associated with clear skies and dry air. The pressure differences are relatively slight, up to about ten percent of atmospheric pressure (Heidorn, 2005).

High and low pressure cells are also characterized by converging and diverging horizontal air movement toward or away from their centres at both surface level and aloft. The convergence or divergence of surface air is responsible for generating vertical motion in the atmosphere. To maintain mass balance, converging winds at the surface are

---

<sup>1</sup> When low or high pressure cells elongate, they are referred to as troughs or ridges, respectively.

off-set by diverging winds aloft (cyclone<sup>1</sup>), creating an upward air movement, and diverging winds at the surface are off-set by converging winds aloft (anticyclone), creating a downward air movement, as shown in Figure 1. Cyclones carry moisture from the surface, causing clouds and precipitation, and are associated with unsettled or *stormy* weather. Conversely, anticyclones compress and warm descending upper level air, making them unlikely to cause clouds and precipitation, and are associated with stable or *fair* weather.

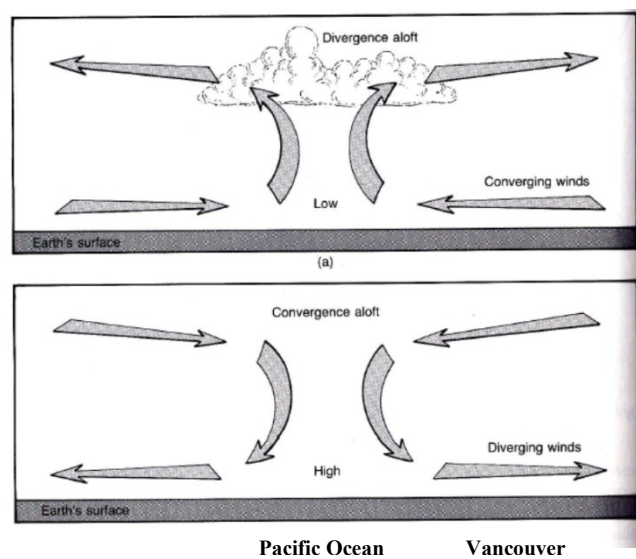


*Figure 1: Schematic diagram showing upward vertical motion and cloud formation associated with converging surface winds and divergence aloft (upper diagram) and diverging surface winds and convergence aloft (lower diagram). Adapted from (Lutgens & Tarbuck, 1989).*

During winter months in the northern hemisphere, circulation over the oceans is predominantly influenced by two intense cyclones, the *Aleutian* and *Icelandic* lows (Lutgens & Tarbuck, 1989). Aleutian lows—which have a particularly significant impact

<sup>1</sup> The *low* pressure centres are called cyclones, and the flow around them, which is in the same direction as the rotation of the earth in the northern hemisphere, is referred to as cyclonic flow; the *high* pressure centres are called anticyclones, and the flow around them, which is opposite to the rotation of the earth, is referred to as anticyclonic flow.



on coastal British Columbia's weather—form when polar maritime air masses drift from their origin off of the Aleutian Islands of Alaska and collide with air masses<sup>1</sup> from other source regions with markedly different thermal and moisture characteristics (Oke & Hay, 1998). Polar Maritime air masses are characteristically very cool, moderately moist, and in the North American context, are responsible for bringing cloudy, damp weather to the Pacific Northwest and coastal British Columbia (Heidorn, 2001).

Embedded in the prevailing westerlies and shifting with the meandering jet stream, these persistent cyclonic lows<sup>2</sup> lead to surface level convergence toward the centre of the cell, typically located off of the west coast of British Columbia, which in turn leads to lifting of the air and subsequent cloud formation. Divergence aloft carries the cloud westward, where precipitation may occur over land to the west, including the Metro Vancouver region. Combined with topographical influences, these systems, which typically last from 3 to 5 days, produce winds from the east to southeast, with a secondary maximum from the northwest. This tendency is related to the combination of the passage of frontal storms, persistent offshore low pressure, and the channeling influence of the NW-SE orientation of the Strait of Georgia on air flows (Oke & Hay, 1998).

### *2.1.3 Sea/land breeze and valley/mountain wind*

Sea and land breezes are caused by diurnal variations in atmospheric pressure resulting from temperature gradients across the division between water and land. After sunrise, temperatures over land rise more quickly than over water. As the temperature of

---

<sup>1</sup> An air mass is an accumulation of air in the atmosphere with approximately constant horizontal temperature and moisture content formed over a period of days or weeks and covering hundreds or thousands of kilometres. (Heidorn, 2001).

<sup>2</sup> Maunder (1968) found that lows over the study period of 1964 to 1965 were dominant for 72% of days (Oke & Hay, 1998).

air above the land area increases, convective currents cause the air to ascend while cooler air over the adjacent water moves inland, creating a *sea breeze*. Sea breezes, which may have a depth of up to several kilometres and extend up to 30 kilometres inland, generally develop several hours after sunrise and peak in the afternoon (Hidore & Oliver, 1993). Land breezes, which are not as well developed as sea breezes, work in reverse—causing a flow back toward the sea at night after the land has cooled but the sea remains relatively warm.

Valley and mountain winds form under circumstances similar to those for sea and land breezes. After sunrise, air moves up the sides of valleys and mountains as day time sun raises the temperature of their slopes. Called *valley winds* because they originate in the valleys (much as winds are called westerlies because they come from the west), they can be responsible for cloud formation over hills and mountains. At night when the slopes cool, the process is reversed and so-called *mountain winds* travel down the slopes back into the valleys.

In Metro Vancouver, sea/land breeze and mountain/valley wind influences are more significant in the summer months when regional circulations are light. The two systems cause air movements in the same direction, inland at low elevations during the day with corresponding outflows aloft (resulting in a circulatory behaviour), and the reverse at night (Figure 2).

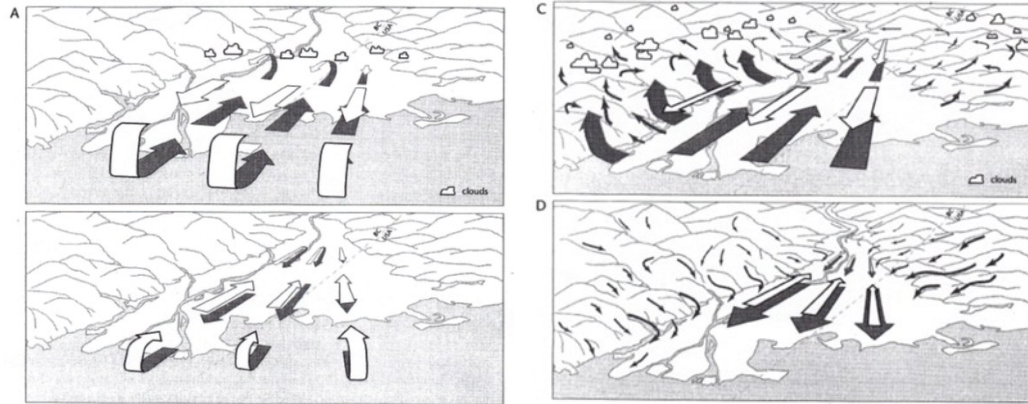


*Figure 2: Schematic diagram showing sea/land breezes over Vancouver during the day (A) and at night (B); and valley/mountain winds during the day (C) and at night (D) (Oke & Hay, 1998)*

#### 2.1.4 Mean annual precipitation and wind

Mean annual precipitation and wind speeds and directions are shown in Figure 3 and Figure 4. Annual precipitation varies over the region from a minimum of about 1.2 m in the south near the airport and Canada-USA boarder to a maximum of about 2.5 m in the northern part of the region, particularly the upper levels of the North Shore Mountains. Precipitation amounts also increase from the western part of the region to the east, from about 1.2 m near waterfront to about 2.0 m inland. The most densely populated part of the region, near the downtown core, receives about 1.5 m annually on average.

The topographical influences already discussed result in widely varying mean annual wind speeds, from about 1 m/s to 16 m/s over the region. Wind directions are predominantly from the east with some localized exceptions where the wind is observed predominantly from the south and south-east.

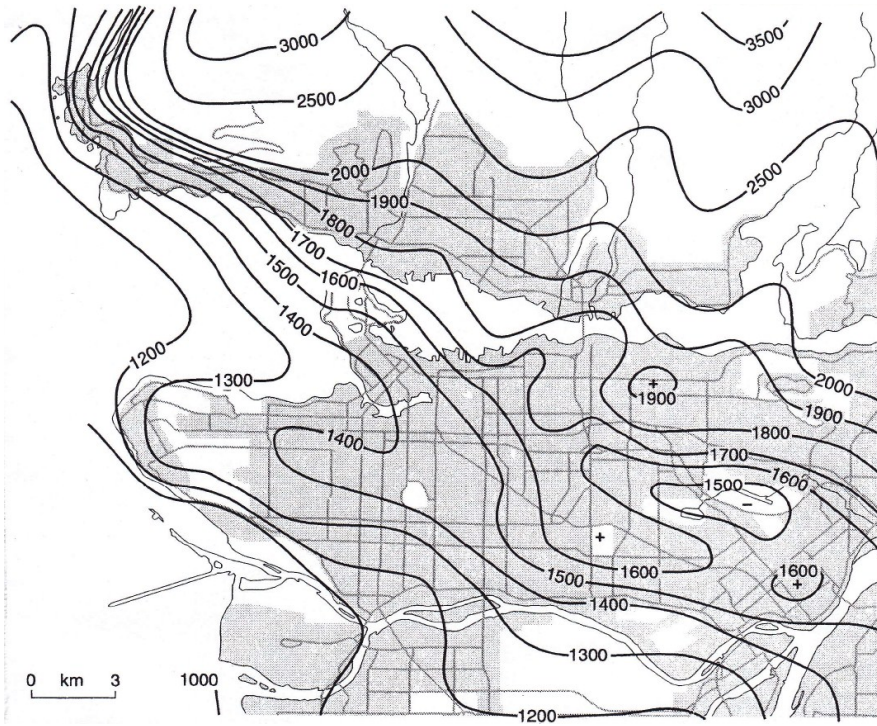


Figure 3: Mean annual precipitation (mm) for Metro Vancouver. Source: (Oke & Hay, 1998).

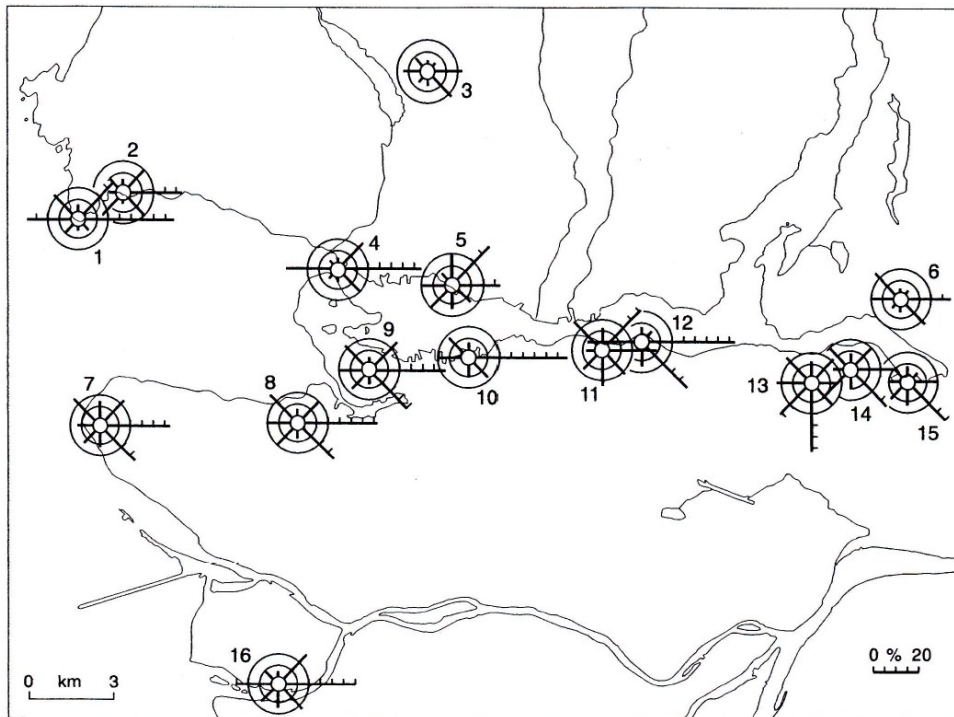


Figure 4: Mean annual wind speed and direction for Metro Vancouver. Source: (Oke & Hay, 1998).

## 2.2 Fundamentals of wind and rain

Buildings lie within the atmospheric boundary layer and are exposed to winds that are perturbed by their presence. The flow, which may be laminar or turbulent, has an impact on raindrop trajectories and rain wetting, which in turn influences wind-driven rain. In this section, fundamental concepts of wind and rain that may aid in the understanding of wind and rain on buildings are reviewed.

### 2.2.1 *Wind*

This section begins with a review of laminar flow and turbulence. The atmospheric boundary layer is defined, including a description of its development and characteristics of its velocity profile. The section ends with a description of air flow patterns around buildings.

#### 2.2.1.1 *Laminar flow*

Under steady, laminar flow, imaginary *streamlines* can be drawn tangential to the direction of flow, as show in Figure 5. The streamlines form the boundaries of virtual steam tubes, through which conservation of mass and energy (Bernoulli's equation) apply at planes 1 and 2 normal to the direction of flow:

$$\rho_1 \cdot A_1 \cdot u_1 = \rho_2 \cdot A_2 \cdot u_2 \quad (2.1)$$

where  $\rho$  is the mass density of the fluid,  $A$  is the transverse area of the stream tube, and  $u$  is the velocity across the steam tube. For incompressible flow,

$$Q = A_1 \cdot u_1 = A_2 \cdot u_2 \quad (2.2)$$

where  $Q$  is the volumetric flow rate through the steam tube. And for conservation of energy,

$$p_1 + \frac{1}{2} \cdot \rho_1 \cdot u_1^2 + \rho_1 \cdot g \cdot z_1 = p_2 + \frac{1}{2} \cdot \rho_2 \cdot u_2^2 + \rho_2 \cdot g \cdot z_2 \quad (2.3)$$

where  $p$  is pressure,  $g$  is gravitational acceleration, and  $z$  is height above a reference plane.

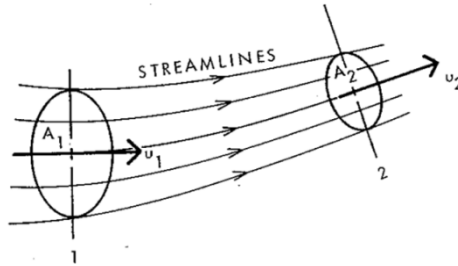


*Figure 5: Stream tubes delineated by stream lines showing velocity and transverse area through which conservation of mass and energy apply (Hucheon & Handegord, 1989)*

#### 2.2.1.2 Turbulence

At high enough Reynolds numbers, a small perturbation in laminar flow will become unstable as the constrained stream tube experiences increased velocity. As predicted by Bernoulli's equation, the increased velocity in the constrained stream tube tends to further contract the tube (Figure 6). The initial perturbation crests into a vortex as a second perturbation is initiated (Figure 8). The two vortices may interact, one vortex inducing a velocity at the other, they may form pairs (Figure 7), or depending on their respective sense, they may rotate around one another or join together. Vortices form over a range of eddy size inversely proportional to viscosity (Panton, 1996).

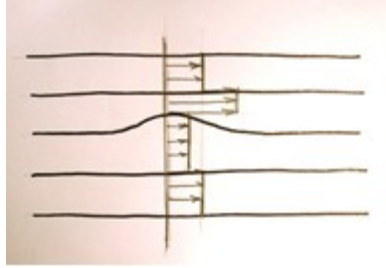


*Figure 6: Perturbation in otherwise laminar flow showing increased velocity in constrained stream tube*

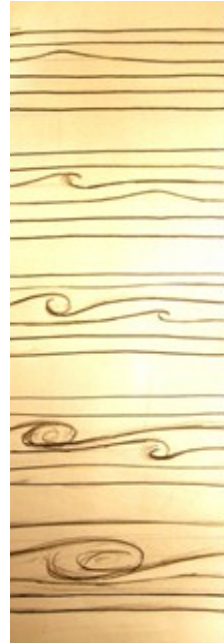


*Figure 8: Path to Chaos from perturbation (top) to vortex interaction*



*Figure 7: Sketch depicting the appearance of vortex pairing showing downstream eddies as larger and fewer in number*

Turbulent flow is chaotic and, except for the mean flow, is irreproducible. As fully turbulent flow develops, vortices evolve over a length scale of up to six orders of magnitude creating a mechanism that cascades energy to smaller and smaller eddies until it is dissipated at the Kolmogorov scale. The extraordinary range of scale engaged in the physical behaviour of turbulence makes full field calculations impossible. Although no general theory is available to describe turbulence for all boundary conditions, universal theories may be possible in structured classes, such as boundary layer turbulence, shear layer instabilities, and turbulent jets. The atmospheric boundary layer is one such structured class of turbulence and has specific applications in the study of wind and buildings.

### 2.2.1.3 *Atmospheric boundary layer*

At the interface between an immersed body and a moving fluid, there is no relative motion between the fluid and the solid. The velocity increases from zero and approaches the main stream velocity asymptotically at some distance from the surface. The region over which the velocity is less than the main stream velocity is termed the boundary layer. For convenience, the thickness of the boundary layer is defined as the locus of points where the velocity  $u$  parallel to the plate reaches 99 percent of the external velocity  $U$  (White, 2008). The boundary layer can be thought of as the region of flow over which the velocity profile is affected by the bounding surface. It can be as thin as a few hundredths of a millimetre (White, 2008) or, in the case of the atmospheric boundary layer, as thick as several hundred metres or more (Hucheson & Handegord, 1989).

The case of a thin flat plate oriented parallel to the direction of flow presents a convenient case for describing development of a boundary layer. As shown in Figure 9, the velocity of the fluid is influenced by viscous forces at the surface of the plate. The boundary layer forms at the leading edge of the plate. It increases in thickness downstream of the leading edge until, at some point, the flow begins to transition from laminar to turbulent. The thickness of the boundary layer increases sharply through this transition range until fully turbulent flow is developed.



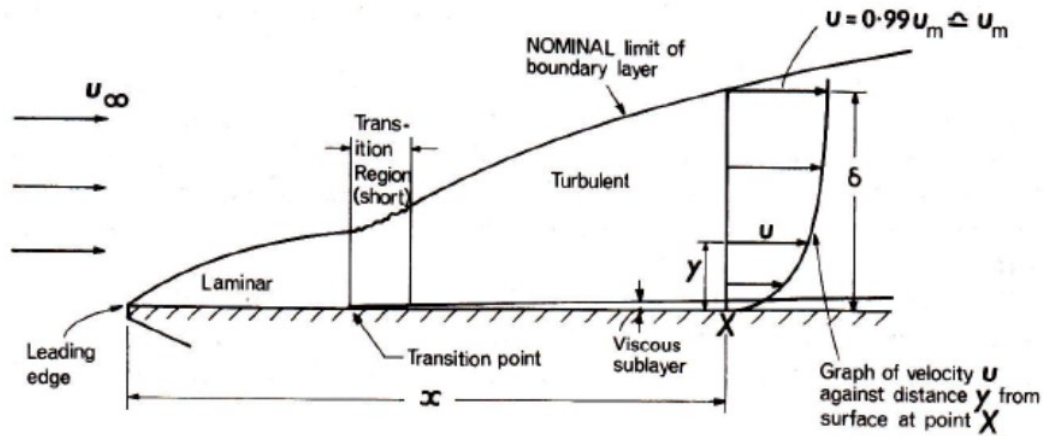


Figure 9: Development of a turbulent boundary layer on a flat plate (Massey, 1979)

Dimensionless velocity profiles under turbulent flow can be approximated by the one-seventh power law<sup>1</sup>.

$$\left(\frac{u}{U}\right)_{turb} \approx \left(\frac{y}{\delta}\right)^{1/7} \quad (2.4)$$

where  $(u/U)_{turb}$  is the dimensionless velocity profile under turbulent flow,  $y$  is distance from the bounding surface, and  $\delta$  is the thickness of the boundary layer.

In the case of the earth's atmospheric boundary layer, the 1/7 power law reasonably describes wind profiles over flat, open country but may better reflect profiles over rougher surfaces, such as over cities, with a larger exponent—up to about 1/2 for the centres of large cities (Hucheon & Handegord, 1989). The mean wind speed  $V_z$  at height  $Z$  is given by

$$\frac{V_z}{V_g} = \left[\frac{Z}{Z_g}\right]^\alpha \quad (2.5)$$

<sup>1</sup> Hucheon and Handegord (1989) attribute this well-known relationship to von Karman while White (2008) attributes the same expression to Prandtl.

where  $V_g$  is the mean gradient wind speed corresponding to the velocity at the outer limit of a boundary layer with a thickness  $Z_g$ . The exponent  $\alpha$  varies with roughness from as low as 0.1 for open sea to as high as 0.4 for city centres (Hutcheon & Handegord, 1989). The boundary layers range in height from 250 to 500 m.

A power law can also represent the variation of gust speed with height:

$$\frac{G_z}{G_g} = \left[ \frac{Z}{Z_g} \right]^\beta \quad (2.6)$$

where

$$G_g = 1.35V_g \quad (2.7)$$

and  $G_z$  is the peak or gust speed at height  $Z$ ;  $G_g$  is the peak or gust speed at gradient height  $Z_g$ , and  $\beta$  is an exponent related to terrain roughness with a value of about  $0.6\alpha$ .

Like  $\alpha$  and the gradient height  $Z_g$ , the exponent  $\beta$  varies with terrain roughness. Hutcheon and Handegord (1989) list values of  $\alpha$  and  $\beta$  for four different terrain categories ranging from open sea to city centres. The mean wind speed is shown to drop markedly with increased terrain roughness at heights of up to 100 m. When wind information is available for one site, such as an airport, the expressions may be applied to predict the wind conditions at another site, such as a city centre, by first determining the mean and peak wind speeds at gradient height (assuming that the mean gradient wind speed is similar at the two sites).

#### 2.2.1.4 Airflow around buildings

Airflow around buildings (Figure 11) typically involves a frontal vortex, separation at building corners, corner streams, recirculation zones, shear layers, and a far

wake (American Society of Heating, Refrigerating, and Air-Conditioning Engineers, Inc., 2009).



*Figure 10: Air flow patterns around a rectangular building, including a depiction of the frontal vortex and recirculation zones (American Society of Heating, Refrigerating, and Air-Conditioning Engineers, Inc., 2009)*

The frontal vortex is transverse to the main flow at the windward wall, and as it wraps around the side of the building, it falls into alignment with the large velocity in the main stream direction and is stressed as a result. The resulting strain intensifies the vortex, creating corner streams of intense vortices (Abernathy, 1968; Panton, 1996; Tennekes & Lumley, 1972).

The flow patterns shown in Figure 11 also involve boundary layer separation and recirculation as well as shear layer instabilities. Generally, the flow velocity near the surface of any object in a wind flow field decreases as the boundary layer grows. Separation of flow, such as over uneven surfaces or at the corners of buildings, occurs when the velocity gradient drops to zero, as shown in Figure 11. The flow beyond the

point of separation is reversed, resulting in a recirculation zone downwind of the point of separation and above the surface to where the velocity gradient drops to zero.

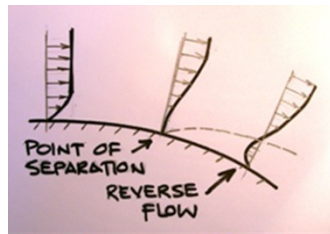


*Figure 11: Boundary layer separation, such as at building corners*

Shear-layer instabilities may develop when two uniform streams of differing velocities, one fast moving and one slow moving, meet downstream from a plate such that the age of the resulting perturbation increases in the downstream direction (Figure 12).

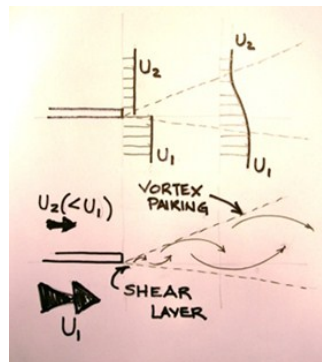


*Figure 12: Sketch of a shear layer at the end of a plate separating fluids with a velocity difference*

If a disturbance causes a large enough displacement of the resulting slip surface to be unstable, the displacement will increase exponentially with time and move with the average speed of the main flow. This instability exhibits vortex pairing behaviour and is common in the downwind wakes that trail from the corners of buildings. Large eddies become larger by entraining fluid outside the shear layer and by vortex pairing (Panton,

1996). Vortex pairing may also occur downwind of a building when the two streams that form around the building reunite on the lee side of the building.

The frontal vortex is an important influence on wetting patterns resulting from wind-driven rain, particularly on the windward wall. Figure 13 depicts the development of a typical wind-driven rain wetting pattern on the walls of a high rise building over time. The frontal vortex entrains raindrops, altering their trajectories and resulting in a concentration of wetting along the top edge and at the upper corners, as shown in the figure. Raindrops entrained in the frontal vortex may also impinge on vertical projections from the wall surface, such as mullions on a high rise building or other object that projects outward from the field of the wall, creating concentrations of wetting directly below the projection.

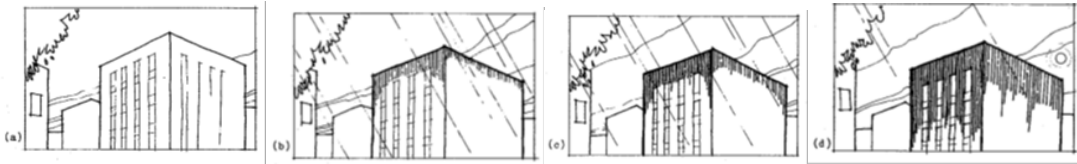


*Figure 13: Typical wetting patterns on a high rise building exposed to wind-driven rain over time showing concentrations along the top edge and at the upper corners of the windward wall (Robinson & Baker, 1975)*

The wind flow field around buildings also influences wind pressures on the building surface. Wind pressures at various locations on a building surface are expressed in terms of the pressure coefficient,  $C_p$ , the ratio of the actual pressure measured (or expected) at a particular location on the surface of the building to the theoretical stagnation pressure. The pressure coefficient is given by

$$C_p = \frac{p}{\frac{1}{2} \rho \cdot V^2} \quad (2.8)$$

where

$C_p$  is the pressure coefficient,

$p$  is the measured or expected pressure (Pa),

$\rho$  is the density of air ( $\text{kg/m}^3$ ), and

$V$  is the wind speed at the height of the building (m/s).

The pressure coefficients for the windward wall of a high-rise building corresponding to various wind directions measured from the normal to the wall surface are shown in Figure 14. They range from 0.1 to 0.9, depending on the location on the wall and the wind direction. For wind directions normal to the wall, the pressure coefficient is at its maximum of 0.9 at a location horizontally centred on the wall and at an elevation of about eight tenths of the height of the building. It drops to between 0.6 and 0.7 along the top edge and to less than 0.5 at the upper and lower corners.

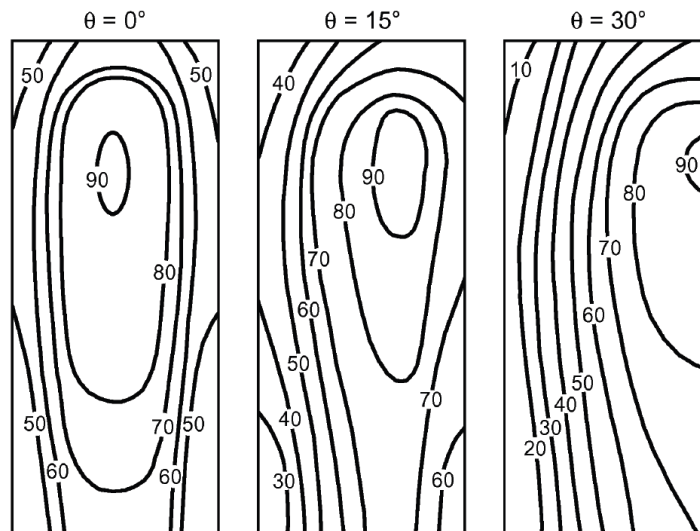


*Figure 14: Local pressure coefficients ( $C_p \times 100$ ) for tall buildings with wind direction at angles of 0, 15, and 30 degrees measured normal to wall surface (American Society of Heating, Refrigerating, and Air-Conditioning Engineers, Inc., 2009)*

As the wind direction shifts from perpendicular, the location of maximum pressure coefficient also shifts. At 15 degrees to the normal, the maximum coefficient is still 0.9, but its location shifts toward the windward edge while pressure coefficient at the leeward

edge drops to less than 0.4. At 30 degrees to the normal, the maximum coefficient of 0.9 occurs at the windward edge, and at the leeward edge, the coefficient drops to less than 0.1.

The pressure coefficients for the windward wall of a low-rise building are shown in Figure 15. They range from 0 to 0.8. For wind directions normal to the wall, the maximum coefficient is greater than 0.8 and is centred on the upper edge of the wall. The coefficient drops to less than 0.5 at the lower corners. When the wind direction is at 45 degrees to the perpendicular to the wall, the location of maximum pressure coefficient shifts toward the wind but drops to between 0.5 and 0.7. As shown in the figure, the pressure coefficient may be less than zero at the lower leeward corner in low rise buildings when the wind direction is at 45 degrees to the normal.

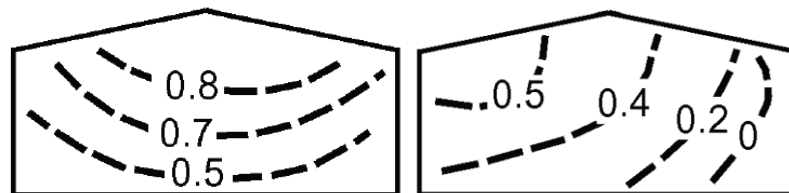


*Figure 15: Local pressure coefficients for the windward wall of a low-rise building with wind direction normal to surface (left) and at 45 degrees to the normal (American Society of Heating, Refrigerating, and Air-Conditioning Engineers, Inc., 2009)*

### 2.2.2 Rain

This section reviews the fundamentals of rain beginning with rain formation and drop size distribution. Definitions are given for rainfall intensity, the rain intensity vector, the terminal fall speed of raindrops and free wind-driven rain. Measurement methods for horizontal and wind-driven rain are reviewed, and the section ends with an overview of the concept of catch ratio.

### *2.2.2.1 Rain formation and raindrop size distribution*

Condensation of water vapour onto nuclei creates cloud droplets, their formation aided by cooling from buoyancy-induced upward air movement. The droplets, ranging in diameter from 1 to 50 micrometres, are suspended in the air and follow the air movement. They generally maintain a spherical shape because the forces of surface tension exceed those of aerodynamics and gravity. Drops form on nuclei within clouds and can grow quickly under ideal conditions. Above diameters of 0.10 to 0.25 mm, they begin to fall against air movement and melt as they pass through warmer altitudes. Raindrops may coalesce into larger drops, which fall faster and coalesce into still larger drops with increasing frequency. A drop may become so large that aerodynamic forces overcome surface tension forces, which results in the drop breaking apart. Drops larger than about 6 to 7 mm are unstable. Raindrops are increasingly likely to coalesce under increasingly intense rainfall. The distribution of raindrop sizes depends on rainfall intensity, type of storm, cloud height, and other factors. Relationships between drop diameter and terminal velocity can be predicted as described in Section 2.2.2.3. Raindrops with diameters above 0.28 mm lose their spherical shape and become oblate spheroids<sup>1</sup> (Blocken & Carmeliet, 2005).

Best (1950) derived an expression for relative probability distribution of raindrop diameter as a function of rainfall intensity. He based his results on experimental data collected primarily by exposing dye-impregnated, absorbent paper to rain in order to count, measure, and calibrate the water-stains in terms of drop size. As an alternative method, he also exposed pans of sifted flour to rain in order to retrieve, bake, and evaluate the pellets formed by contact of the raindrops with the flour. He derived an

---

<sup>1</sup> Raindrops are not tear-shaped, as they are often illustrated graphically.



expression for the fraction of water in air comprising drops of less than a specific diameter as a function of the rainfall intensity. Noting that raindrop size distribution is related to many factors—such as rate of rainfall, type of rain (such as continuous, thunderstorm, or orographic), position relative to centre of the rainstorm, and relative humidity—the author takes a simplified approach considering only rate of rainfall as an influence on average drop size distribution. The drop size distribution at ground differs from that of the distribution in air because of the influence of drop size on terminal velocity. While the Best's measurements were taken at ground level, he presents results for the size distribution in air by dividing the terminal velocity into the number of drops of a particular size at ground level.

#### 2.2.2.2 *Rainfall intensity and the rain intensity vector*

The flux density of liquid water at a point in the flow field during a rain event is termed the *rainfall intensity* and has units of litres per second per square metre ( $\text{L}/\text{s}\cdot\text{m}^2$ ). It can be thought of as the quotient of the rate of liquid water flow through an aperture in litres per second ( $\text{L}/\text{s}$ ) and the area of aperture. Rainfall intensity is frequently measured using a rain gauge placed with its aperture oriented horizontally. The rate of catch of liquid water in a rain gauge is typically expressed in millimetres of accumulation<sup>1</sup> on a horizontal plane per hour ( $\text{mm}/\text{h}$ ) and is termed the *horizontal rainfall intensity*. The intensity at a particular moment is determined by the rate of fall based on the shortest practical measurement period (Environment Canada, 1997).

Rain flux density can also be measured using a gauge with its aperture oriented vertically. In the absence of wind (i.e. assuming still air), the raindrop trajectories are vertical and the catch in a vertical gauge would be zero. Wind causing horizontal air

---

<sup>1</sup> Note that 1 mm of accumulation on a horizontal plain is equivalent to 1  $\text{L}/\text{m}^2$ .

movement, however, imparts a horizontal component to the velocity of each raindrop, the magnitude of which depends on the diameter of the raindrop, and results in oblique raindrop trajectories. Rain that is given a horizontal velocity component by the wind in this way is termed *wind-driven rain* and may also be referred to as *driving rain* (Blocken & Carmeliet, 2004). The rain flux density at a point centred on a vertical aperture is termed the *wind-driven rain intensity*.

Together, the orthogonally oriented horizontal rainfall intensity and wind-driven rain intensity form the components of the *rain intensity vector*, as shown in Figure 16.

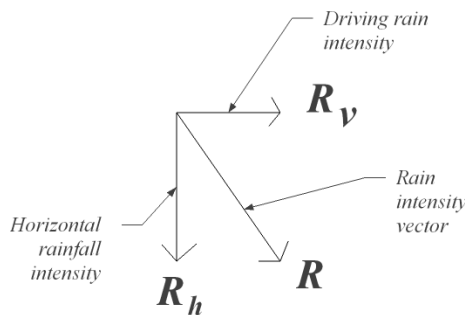


*Figure 16: The rain intensity vector with its components of horizontal rainfall intensity and driving rain intensity adapted from Blocken and Carmeliet (2004).*

The rain intensity vector is the magnitude and direction of maximum intensity of rainfall. *Driving rain intensity* can be defined as the "component of the rain intensity vector causing rain flux through a vertical plane". According to Blocken and Carmeliet—who quote this definition in their extensive review of wind-driven rain (2004)—the International Council for Building Research (CIB) has adopted this definition.

The term *wind-driven rain* takes on a narrower meaning with respect to measurements on vertical building surfaces, as described in Section 2.2.2.6. To differentiate between wind-driven rain impinging on a building surface and wind-driven rain passing through an imaginary aperture in an unperturbed wind flow field, the latter is often referred to as being *free* of obstructions and leads to various associated nomenclature, such as in *free field wind-driven rain*, *free field conditions*, or a *free-standing rain gauge*, all of which imply that the associated wind flow field is unperturbed.

For qualitative purposes, the Manual of Surface Weather Observations (MANOBS) provides a guide for judging rainfall intensity visually without the aid of instruments, as shown in Table 1 below.

*Table 1: MANOBS guide for determining the intensity of rain visually without the aid of instrument measurements (Environment Canada, 1997).*

	<b>Light Rain</b>	<b>Moderate Rain</b>	<b>Heavy Rain</b>
Individual drops	Easily seen	Not easily seen	Not identifiable (rain in sheets)
Spray over hard surface	Hardly any	Noticeable	Heavy to a height of several centimetres
Puddles	Form slowly	Form rapidly	Form very rapidly

### 2.2.2.3 Terminal fall speed of raindrops

Dingle and Lee (1972) developed an expression for terminal velocity of raindrops falling in still air as a function of diameter. Based on a regression analysis of measurements by Gunn and Kinzer (1949), the authors developed a single expression relating drop radius to terminal fall speed (rather than having multiple equations cover a full range of drop sizes, e.g. from 0.1 mm to 5.8 mm):

$$v_T = -16.6033 + 491.8441d - 88.8016d^2 + 5.4888d^3 \quad (2.9)$$

$$0.1 \leq d \leq 5.8 \text{ mm}$$

where  $v_T$  is the terminal fall speed of raindrops in still air (cm/s) and  $d$  is the diameter of the water drop (mm). The diameter of a non-spherical water drop is taken as the diameter of a spherical water drop with an equivalent mass.

The authors compared drag forces for water drops and rigid spheres and found that at diameters above about 1 mm the water drops developed a higher drag force, such that water drops fall more slowly than an equal-massed rigid sphere. Below 1 mm, circulation in the water drops induced by friction reduces the slip-velocity such that these drops fall faster than equal mass rigid spheres (McDonald, 1954)<sup>1</sup>. Above about 1.4 mm, drop distortion and vortex shedding further influence the terminal velocity. For large drop sizes, the concept of terminal velocity may be inappropriate because the range and frequency of oscillation of fall speed become increasingly significant (i.e. the fall speed for a given size of drop cannot be expressed as a single value).

#### 2.2.2.4 *Horizontal wind and intensity of free wind-driven rain*

For idealized steady-state conditions of uniform horizontal wind and a single raindrop diameter (and therefore single terminal velocity for all raindrops), the horizontal component of velocity of each raindrop can be assumed to be equal to the horizontal wind speed; and the vertical component of velocity of each drop, to its terminal fall speed in still air, this latter assumption a reasonable one because raindrops reach a terminal uniform velocity within only a few metres (McDonald, 1954). Under these assumptions, the oblique trajectory of each raindrop can then be computed based on its diameter and

---

<sup>1</sup> This article is based on *Theoretical cloud physics studies*, Final report on Contract Nonr757, Project No. NRO82093. Office of Naval Research, January 31, 1953.

the wind speed, as shown in Figure 17, and the theoretical intensity of free wind-driven rain—or driving rain—becomes the product of the horizontal rainfall intensity and the ratio of horizontal wind speed to terminal velocity of the raindrops:

$$R_v = R_h \cdot \frac{U}{v_t} \quad (2.10)$$

where

$R_v$  = driving rain intensity (mm/h or L/h·m<sup>2</sup>),

$R_h$  = horizontal rainfall intensity (mm/h or L/h·m<sup>2</sup>),

$U$  = wind speed (m/s), and

$v_t$  = raindrop terminal velocity (m/s).

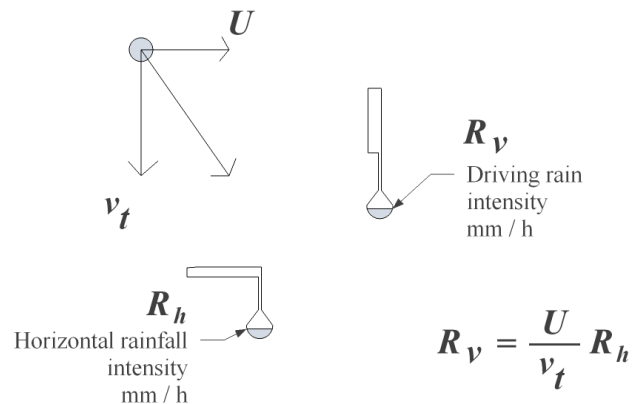


*Figure 17: The relationship between horizontal rainfall intensity and driving rain intensity under idealized conditions of steady, uniform and horizontal wind and a single raindrop diameter*

#### 2.2.2.5 Measurements of horizontal rain

The quantity of measured rainfall is typically expressed in terms of vertical depth of water in millimetres (mm) collected over a specific period of time (Environment Canada, 1997). Measurements are most commonly taken with a gauge consisting of a right-sided cylinder attached to a funnel, referred to as a *standard rain gauge*. The aperture of a standard gauge is placed in a horizontal orientation at an elevation of

between 0.5 and 1.5 m, and either the volume or weight of accumulated water is measured (World Meteorological Organization, 2008)<sup>1</sup>. The Meteorological Service of Canada (MSC) standard rain gauge (Type B) is a cylindrical container with a height of 400 mm high and 113 mm in diameter, with precipitation funnelled into a plastic cylinder marked with graduations for measurement. The body of the gauge can disrupt the wind flow field in the vicinity near the gauge causing a change in the trajectories of raindrops and introducing a potential measurement error. Blocken and Carmeliet (2005) proposed a method of reducing this error by building a sloped earthen embankment around the gauge to an elevation matching the elevation of the horizontal aperture.

Automated measurements are also frequently made with a tipping bucket rain gauge, with data fed to an electronic acquisition system. A standard rain gauge can be used in conjunction with a tipping bucket rain gauge to establish correction factors for the tipping bucket gauge (Environment Canada, 1977). Precipitation amounts of 0.2 mm or less are considered difficult to measure and are recorded as a “trace” amount or 0.2 mm (e.g. the amount 0.1 mm is not recorded).

Automated measurements can also be made with a capacitance rain gauge consisting of a cylindrical collector containing a stainless steel rod covered with polytetrafluoroethylene (PTFE), which in combination with the collected water forms a coaxial capacitor and dielectric (Blocken & Carmeliet, 2005). An increase in rainwater causes the surface area of the capacitor, and hence the capacitance, to increase. The capacitance is measured and converted to an analogue voltage output (Nystuen et al, 1996).

---

<sup>1</sup> Rain intensity measured through a horizontal aperture is termed *horizontal rainfall intensity*.

### 2.2.2.6 Measurements of wind-driven rain

As described in Section 2.2.2.2, wind-driven rain can be measured in two locations: 1) on buildings with gauges placed directly on wall surfaces to measure wind-driven rain loads and 2) under free field conditions with gauges placed away from the influence of buildings and other obstructions to measure so-called *free wind-driven rain*<sup>1</sup>. The former is generally of most interest for wind-driven rain research; the latter is sometimes difficult to achieve in practice because of the nature of surrounding topography and other obstructions typical of urban environments.

Measurements of free wind-driven rain made with a single aperture can indicate temporal distribution of rainfall intensity; however, to establish the magnitude and direction of maximum rain intensity—or in other words, the rain intensity vector—multiple gauges (or a single gauge with multiple apertures) must be used. For example, the rain intensity vector for a particular exposure can be calculated with data collected from two orthogonally placed apertures, as shown schematically in Figure 18.

Free-standing wind-driven rain gauges may include combinations of up to eight vertical apertures and one horizontal (an 8-way gauge versus a 4-way gauge) to obtain directional information. Although most weather stations measure only horizontal rain, some researchers have explored gauges with multiple apertures. In 1936 at the Building Research Station (BRS) in the UK, Beckett employed a gauge with eight vertical apertures and one horizontal aperture (Beckett, 1938; Lacy R. E., 1951; Blocken & Carmeliet, 2004), and in 1937, Holmgren (Holmgren, 1946; Blocken & Carmeliet, 2004) employed a gauge with four apertures at the Norwegian Building Research Institute. Choi (2001) also used a gauge with four apertures and included provisions to allow wind flow

---

<sup>1</sup> The conditions for free wind-driven rain are referred to as *free field* conditions.

through the gauge body to help reduce distortion of the wind flow field caused by the gauge itself. Wind-driven rain gauges for buildings (see below) are now also sometimes used to measure free wind-driven rain in one direction only.

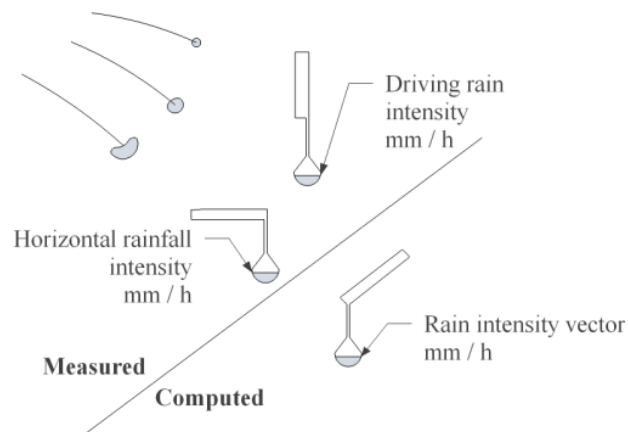


*Figure 18: Schematic diagram with orthogonally oriented apertures measuring horizontal rain intensity and driving rain intensity that can be used to establish the rain intensity vector*

Comparisons of free wind-driven rain gauges were made beginning in 1953 through the CIB (Birkeland, 1963; Blocken & Carmeliet, 2004). Though no standard emerged and wind-driven rain gauges at weather stations are still rare, Blocken and Carmeliet have observed that measurements from various types of directional gauge lead to the consistent conclusion that intensity of free wind-driven rain increases approximately proportionally with wind speed and horizontal rainfall intensity. Other types of rain gauges have also been employed for research purposes, including a vibrating wire, weighing-bucket rain gauge (Duchon, n.d.), and another with an aperture orientation that rotates to match wind direction (Chand & Bhargava, 2001).

Driving rain gauges are also placed on the walls or other vertical surfaces of buildings to measure wind-driven rain impinging on the surface. The most common type is a *plate driving rain gauge* (Figure 19). Use of a driving rain gauge on a building has



been traced back to Holmgren, who used a wind-driven rain gauge in 1937 in Trondheim, Norway (Lacy R. , 1965), and later in 1943 to Nell, who used a wind-driven rain gauge in Voorschoten, the Netherlands (van Mook F. J., 2002). The gauges were plate type consisting of a collection area and reservoir. A recessed plate-type gauge was recommended by the CIB Working Commission on Rain Penetration to minimize disturbance to the wind field around the gauge but has given way to surface mounted gauges for practical ease following reports of only occasional discrepancies between the two (Blocken & Carmeliet, 2004).



*Figure 19: A plate driving rain gauge with circular collection area and concealed tipping bucket recording mechanism (photograph courtesy of National Research Council Canada)*

of up to 100 percent<sup>1</sup>. Simulations of adhesion, coagulation (transformation of a liquid into a soft, semisolid, or solid mass), and run-off for a PVC gauge validated by

Driving rain gauges used by researchers vary in size, shape, material, and recording mechanism, and results from these various gauges can vary widely. The duration, intensity, type of rain event, and the sampling frequency of measurement also affect the results. One of the most significant measurement errors is associated with *adhesion water* (Blocken & Carmeliet, 2005). Adhesion water refers to the individual water droplets and films that do not run-off the collection area of the gauge. Adhesion water can introduce a significant error when it escapes measurement by evaporation. Indications from two studies suggest errors

---

<sup>1</sup> According to Blocken and Carmeliet (2004), special gauges to measure adhesion water—one by Kragh was suspended from a load cell and another by Van Mook employed an automated wiper—have collected up to twice the amount collected by conventional gauges that neglect adhesion water.

experimental data (Blocken & Carmeliet, 2004) shows an adhesion error of 100 percent for spells of wind-driven rain of less than about 0.08 mm (i.e. these spells were not recorded by the gauge). Above this threshold, the absolute error remains about constant while the relative error decreases with the amount of wind-driven rain collected. Contrary to earlier thought on measurement errors, hydrophobic surface finishes increase measurement errors associated with evaporation of adhesion water.

Other error sources considered to be of lesser importance include:

- 1) evaporative losses from reservoirs,
- 2) splashing of raindrops from the collection area,
- 3) condensation on the collection area, and
- 4) wind errors (smaller catches) due to the disturbance of the wind flow by the gauge body (Blocken & Carmeliet, 2005).

Two specially designed gauges (Couper, 1974; Hogberg, Kragh, & van Mook, 1999) with deeply recessed collection areas composed of tilted surfaces to minimize splashing losses showed better performance for high wind speed and heavy rainfall intensities (large raindrops). Conversely, the large collection area was a compromise for evaporative losses important for light to moderate rainfall intensities. Condensation errors are generally considered small, a few tenths of a millimetre from nocturnal infrared loss. Wind errors are thought to increase for sharp wind angles.

In addition to measurements of wind-driven rain on buildings, some research has also been conducted based on wind-tunnel testing (Inculet & Surry, 1995), with the goal of exploring the effects of building height and architectural features on wetting patterns. Rain was simulated in a 4 m high by 5 m wide wind tunnel with an array of nine nozzles

intended to produce a drop-size distribution consistent with the 1:64 length scale used. Water sensitive paper placed on the surfaces of the building models indicated the wetting patterns, which were recorded by photograph for analysis.

#### 2.2.2.7 *Catch ratio and specific catch ratio*

In meteorology, the *catch* is the quantity of rain water received in the collector of a gauge and measured in the reservoir over a particular time period. When two gauges are used over the same time period, the *catch ratio* is the quantity collected in one reservoir divided by the quantity collected in the other. Frequently, the catch ratio refers to the quantity collected in a gauge with a vertical aperture divided by the quantity collected in a gauge with a horizontal aperture. In the practical context of measurements of wind-driven rain on buildings, the catch ratio refers to the ratio of the quantity collected from a gauge with a vertical aperture placed on the vertical surface of a building<sup>1</sup> and the quantity collected from a horizontal gauge placed on the roof of the building (van Mook F. J., 1999) or, if possible, in free-field conditions in the unperturbed wind flow field upwind of the building (Blocken & Carmeliet, 2005).

Other names for catch ratio and specific catch ratio have been used by other researchers. Choi (1998) refers to the *local effect factor*, which is equivalent to specific catch ration, and the *local intensity factor*, which is equivalent to catch ratio. Straube (Straube & Schumacher, 2006) refers to the Rain Deposition Factor (RDF), which is similar to catch ratio referred to by Blocken, but rather than being a ratio of rain deposited on a wall to horizontal rain, the RDF is a ratio of rain deposited on a wall to rain through a vertical plane measured under free-field conditions.

---

<sup>1</sup> The term catch ratio is not universally defined. For example, van Mook et al (1997) use the term to refer to the driving rain catch on the vertical surface of a building divided by the vertical catch in free field conditions.

Blocken and Carmeliet identify six parameters that influence catch ratio<sup>1</sup>:

- 1) building geometry and topography,
- 2) position on the building facade,
- 3) wind speed,
- 4) wind direction,
- 5) horizontal rainfall intensity, and
- 6) horizontal raindrop size distribution.

In theory, the *catch ratio* is the flux through a vertical aperture for a particular time period divided by the flux through a horizontal aperture over the same time period (Blocken & Carmeliet, 2004). For steady conditions, the catch ratio can be taken as the ratio of the wind-driven rain intensity to the horizontal rainfall intensity:

$$\eta = \frac{R_{wdr}}{R_h} \quad (2.11)$$

where

$\eta$  = catch ratio,

$R_{wdr}$  = wind-driven rain intensity, and

$R_h$  = horizontal rainfall intensity.

For non-steady conditions, the instantaneous catch ratio at time  $t$  is given by

$$\eta(t) = \frac{R_{wdr}(t)}{R_h(t)} \quad (2.12)$$

where

$\eta(t)$  = catch ratio at time  $t$ ,

---

<sup>1</sup> In addition to these six parameters, Blocken and Carmeliet also identify turbulent dispersion of raindrops as an additional factor affecting catch ratio.

$R_{wdr}(t)$  = wind-driven rain intensity, and

$R_h(t)$  = horizontal rainfall intensity.

The *specific catch ratio* is related to a particular increment of raindrop diameter, as opposed to the entire spectrum of raindrop diameters. For a particular interval of raindrop diameter, the flux through an aperture<sup>1</sup> placed perpendicular to the corresponding trajectories would be the rain intensity vector for that interval of raindrop diameter. The specific catch ratio is given by the following:

$$\eta_d(d, t) = \frac{R_{wdr}(d, t)}{R_h(d, t)} \quad (2.13)$$

where

$\eta_d(d, t)$  = specific  $\eta$  for raindrop diameter  $d$  at time  $t$ ,

$R_{wdr}(d, t)$  = specific  $R_{wdr}$  intensity for raindrop diameter  $d$  at time  $t$ , and

$R_h(d, t)$  = specific  $R_h$  for raindrop diameter  $d$  and time  $t$ .

For a discrete time step  $[t_j, t_j + \Delta t]$ , the specific catch ratio is

$$\eta_d(d, t_j) = \frac{\int_{t_j}^{t_j + \Delta t} R_{wdr}(d, t) dt}{\int_{t_j}^{t_j + \Delta t} R_h(d, t) dt} = \frac{S_{wdr}(d, t_j)}{S_h(d, t_j)} \quad (2.14)$$

where

$\eta_d(d, t_j) = \eta_d(d, t)$  for time step  $[t_j, t_j + \Delta t]$  for raindrop diameter  $d$ ,

$S_{wdr}(d, t_j) =$  specific driving rain amount for raindrop diameter  $d$ , and

$S_h(d, t_j) =$  specific horizontal rainfall amount for raindrop diameter  $d$ .

---

<sup>1</sup> As Blocken and Carmeliet note (2004), the flux of a particular interval of raindrop diameter is considered hypothetical because of the practical difficulty of measuring the flux of a single interval of diameter.

And the catch ratio for a discrete time step for the entire spectrum of raindrop diameters is

$$\eta_d(t_j) = \frac{\int_{t_j}^{t_j+\Delta t} R_{wdr}(t) dt}{\int_{t_j}^{t_j+\Delta t} R_h(t) dt} = \frac{S_{wdr}(t_j)}{S_h(t_j)} \quad (2.15)$$

where

$\eta_d(t_j)$  = catch ratio for time step  $[t_j, t_j + \Delta t]$  for all raindrop diameters,

$S_{wdr}(t_j)$  = driving rain amount for all raindrop diameters, and

$S_h(t_j)$  = horizontal rainfall amount for all raindrop diameters.

### 2.3 Empirical approaches to quantifying wind-driven rain

Wind-driven rain on buildings has been measured and studied since at least 1937 and has led to a number empirical approaches to quantifying wind-driven rain impinged on the walls of buildings. This section provides an overview of the key developments, beginning with a review of the introduction of driving rain maps in 1955 and the concept of driving rain indices in 1965. The relationship between driving rain intensity, wind speed, and rainfall intensity is also addressed, and the section ends with an overview of the British standard for assessing wind-driven rain exposure for a specific building.

#### 2.3.1 *Driving rain maps and indices*

A progression of some milestones in early wind-driven rain research is provided in Figure 20. The first driving rain maps are credited to Hoppestad who, according to Lacy (1965), established a correlation between wind, rain, and free driving rain (the latter using the four-way gauge developed by Holmgren mentioned in Section 2.2.2.6) at four locations in Norway. Based on the relationship so developed, he computed free driving rain at 70 other locations throughout Norway and published the results in 1955 in the

form of driving rain maps. Following the early efforts of Holmgren, Best, and Hoppestad and based on measurements of driving rain on the walls of buildings in Scotland<sup>1</sup>, Lacy (1965) proposed that the product of annual mean wind speed and rainfall—which he termed an *index of driving rain* and plotted on a map in the manner of Hoppestad—could be used by designers and architects as an indication of the severity of exposure for a proposed building site and by researchers as an indication of appropriate conditions for testing assemblies under simulated driving rain.

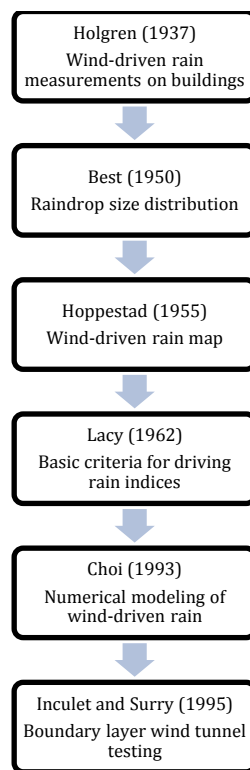


*Figure 20: Progression of some milestones in early wind-driven rain research*

Lacy recognized that the driving rain indices were not a direct indication of the actual amount of driving rain to be expected at a particular location on the wall of a particular

---

<sup>1</sup> Based on Lacy's 1965 paper, the concept of *driving rain index* appears to have been initiated amongst researchers following a paper by Lacy and Shellard (1962), which in turn was based on work by Lacy (1962) at the Garston Building Research Station in Scotland.

building, owing to the influence of the disturbance to air flow caused by the building, and acknowledged also that rain penetration occurs under severe conditions of driving rain rather than the mean annual conditions assumed in computing the index. He concluded, nevertheless, that driving rain maps based on the indices are valid for comparing the severity of exposure at various locations. Lacy's concept of driving rain indices has become the dominant basis for empirical models.

Boyd (1963) and Lacy (1965) extended Lacy's earlier work on the empirical approach by developing driving rain maps for Canada and the U.K. based on indices of annual average values for wind speed and horizontal rainfall amount. The primary contribution is the extension of Lacy's indices to Canada presented in the form of a driving rain map including contours of from 1 to 13 m<sup>2</sup>/s and exposure grades of *sheltered*, *moderate*, and *severe*. The indices and corresponding map were developed from mean annual wind speeds<sup>1</sup> at 175 stations based on observations from 1937 to 1954. Average annual rainfalls for the period 1931 to 1960 were from the Climatology Division of the Meteorological Branch. Rainfall and not precipitation (i.e. including snow) was used. The exposure ratings are apparently consistent with Lacy (1962). Robinson and Baker (1975) later analyzed existing data to generate roses showing occurrences of wind in a specified direction during rain<sup>2</sup>, or in other words, *co-occurrence* of wind and rain. A more recent study on correlation between wind and rain in south western British Columbia showed a significant difference in the wind direction during periods of rain and increased frequency of higher wind speeds during periods of rain (Levelton Engineering,

---

<sup>1</sup> "Climate summaries for selected meteorological stations in Canada", Vol. II (revised), humidity and wind. Department of Transport, Meteorological Branch, Toronto, 1951.

<sup>2</sup> The focus of the paper by Robinson and Baker was to develop a better understanding of weathering and dirt marking.



2006). Of Boyd's work based on mean annual data, Robinson and Baker noted that indices based on monthly or daily values would be even more useful, an approach that was eventually taken in the U.K., to develop a standard for assessing the exposure of walls to wind-driven rain (BS 8104, 1992), as discussed in Section 2.3.3.

Further work (Fazio, Mallidi, & Zhu, 1995) led to improvements based on considering wall orientation. Using thirty years of climatological data for the Montreal region, the authors quantified the driving rain exposure of a vertical surface of a building to establish an index useful in the design of building envelopes by providing the exposure conditions of a vertical wall to rain precipitation as well as rain intensity. The work was extended (Zhu, Mallidi, & Fazio, 1995) to 15 Canadian cities based on hourly mean wind speed using Environment Canada data from airports nearby the cities. To account for the influence of civil infrastructure in urban areas, the authors introduced a surface roughness coefficient (Zhu, Mallidi, & Fazio, 1995) to determine the exposure of a building to driving rain in an urban area based on data from a suburban climatological station.

### 2.3.2 *The relationship between driving rain intensity, wind speed, and rainfall intensity*

As part of an effort to validate his approach to driving rain indices, Lacy (1965) extended the theoretical relationship between horizontal wind and intensity of free wind-driven rain described by Equation (2.10, rewritten here with symbolism used by Blocken and Carmeliet (2004):

$$R_v = R_h \cdot \frac{U}{V_t} \quad (2.16)$$

Because this relationship applies only to a single raindrop diameter, Lacy took the diameter equal to the median raindrop size corresponding to the mean rainfall intensity, based on an empirical relationship proposed by Laws and Parsons (1943), and then

determined the corresponding terminal velocity based on the relationship proposed by Best (1950), arriving at a direct relationship between terminal velocity and rainfall intensity:

$$V_t = 4.505 \cdot R_h^{0.123} \quad (2.17)$$

Combining Equations (2.16) and (2.17) gives the following relationship between driving rain intensity, wind speed, and rainfall intensity:

$$R_v = 0.222 \cdot U \cdot R_h^{0.88} \approx 0.222 \cdot U \cdot R_h \quad (2.18)$$

The constant 0.222, which has units of s/m and is known as the *free driving rain coefficient* (Blocken, Hens, & Carmeliet, 2002) or—in a modified form—as the *driving rain factor* (Straube & Burnett, 1997), implies that the terminal velocity of the drops is  $1/0.222 = 4.5$  m/s. The expression is often simplified by taking the exponent equal to 1. The free driving rain coefficient has been modified to account for the amount of rain impinging on a vertical building surface and for wind directions other than perpendicular to the surface based on a *cosine projection*:

$$R_{wdr} = \alpha \cdot U \cdot R_h \cdot \cos\theta \quad (2.19)$$

where

$R_{wdr}$  = driving rain (or wind-driven rain) intensity on the surface of a wall,

$\alpha$  = driving rain coefficient, and

$\theta$  = angle between the wind direction and the normal to the wall.

Using Computational Fluid Dynamic (CFD) simulations, Blocken and Carmeliet (2004) have shown the cosine projection to be unreliable in predicting the influence of wind direction on the quantity of wind-driven rain.

Straube and Burnett (1997) introduced the Driving Rain Factor (DRF), which is the ratio of rain on a vertical plane (driving rain) to rain on a horizontal plane. The DRF is similar to the proportionality constant in Lacy's equation for the driving rain relationship—which is the inverse of the terminal raindrop velocity. Straube and Burnett (2000) also proposed the Rain Admittance Factor (RAF), a factor to transform the wind-driven rain through a free field vertical plane to that deposited on an actual building. The RAF<sup>1</sup>—a term chosen for consistency with the wind engineering factor *aerodynamic admittance*—accounts for the effect of two types of building geometries, though it neglects the influence of microenvironment<sup>2</sup>.

### 2.3.3 *British standard*

The concept of driving rain indices led to the British Standard BS 8104<sup>3</sup> (British Standards Institution, 1992), which prescribes a detailed procedure to assess wind-driven rain exposure for a specific building. The procedure involves quantifying the wind-driven rain on a specific wall surface using meteorological data measured at weather stations and by introducing four empirical factors: terrain roughness, local topography, obstructions, and building geometry. The standard, which is applicable to low-rise residential buildings in areas other than mountainous regions, presents two methods—the spell index method and annual index method—for assessing exposure of walls of

---

<sup>1</sup> For figures showing RAF (i.e. elevation views of three buildings including low-rise buildings with flat and peaked roofs and a tall building) as contour lines on the building surface refer to Institute for Research in Construction, National Research Council report on MEWS, Task 4, Environmental conditions final report (Cornick, Dalgliesh, Said, Djebbar, Tariku, & Kumaran, 2002).

<sup>2</sup> The general approach by Straube for quantifying wind-driven rain on buildings is described in the text book he co-authored with Burnett (Straube & Burnett, 2005).

<sup>3</sup> The standard BS 8104 was the basis for the European Standard PrEN 13013 (European Committee for Standardization, 1997) and International Standard ISO TC 163/SC 2 N (International Organization for Standardization, 2005).

buildings to wind-driven rain for peak and average conditions respectively. A *spell* is a period or sequence of periods of wind-driven rain intended to reflect peak conditions while the annual index reflects average conditions over an entire year. Generally, the annual average index is suitable when average conditions are important—for the hygrothermal analysis or testing of masonry, for example—and the spell index is suitable when peak conditions are important—such as when predicting rain penetration at a crack.

An index is generally determined for airfield conditions, a hypothetical quantity of driving rain that would occur at 10 m above ground in an open field at the location of the proposed wall, and then modified by multipliers to arrive at the wall index, either the wall annual index or wall spell index. The airfield index is determined by using a combination of maps and roses. The maps indicate contour intervals for geographical increment and are also divided into regions and sub regions. A spell rose and annual rose are then provided for each region. The airfield indices (both spell and annual indices) for a particular location are determined by reading the geographical increment from the map, reading the rose value for the appropriate sub region and direction, summing the two to determine a "map value", and then finally either computing the airfield indices by formula based on the map value (one for each of spell and annual index) or looking up values in tables based on the formulas.

Correction factors to the airfield index are made for terrain roughness, topography, obstructions, and wall characteristics--including roof overhang. The terrain roughness factor accounts for the average height and spacing of protective features such as buildings and trees as well as the presence of coasts or estuaries within 8 km and is determined by comparing actual conditions with categorical descriptions (a simple table

summarizes the categories). The topography accounts for the effect of marked changes in ground level within 1 km upwind caused by hills, cliffs, etc. on wind speed (the map values already account for the height above sea-level) and is determined by a simple table (three values of 0.8, 1.0, or 1.2) when the land does not slope away from the wall at more than 1 in 20 or by a presumably more involved method when the slope exceeds 1 in 20. The obstruction factor accounts for buildings, fences, trees, and other windward objects that are near to (within 120 metres based on the range of factors shown in the table) and shelter the wall and are within a line of sight of up to 25 degrees from normal in either direction. The wall factor accounts for characteristics of the geometry of the building and is expressed as the catch ratio for various sizes of building, roof type, and position on wall.

#### 2.4 Test standards and parameters for window testing

Testing of window assemblies is conducted by spraying a known quantity of water on the outside surface while applying a static pressure differential across the assembly. The air pressure may also be cycled on-and-off to simulate fluctuating wind pressures. A window passes the test if no water causes wetting of the interior room surfaces, no water passes through the window into the wall below the window sill, and no water remains trapped in the window assembly upon removal of the air pressure at the end of the test.

In addition to providing quality assurance at manufacturing plants and in the field, the tests are used in certification programs, such as the CSA Windows & Doors Certification Program, the Canadian Construction Materials Centre (CCMC) Doors and Windows Evaluation Program, and the Window-Wise Certification program (RDH

Building Engineering, 2002). Certification typically involves testing to CSA A440 standards by a third party agency recognized by the certifying body.

Typical test set-ups (Figure 21) generally involve a chamber with an opening to install the test assembly, a means of applying a known air pressure differential across the assembly, and a device able to spray a known quantity of water uniformly over the outside surface of the assembly.

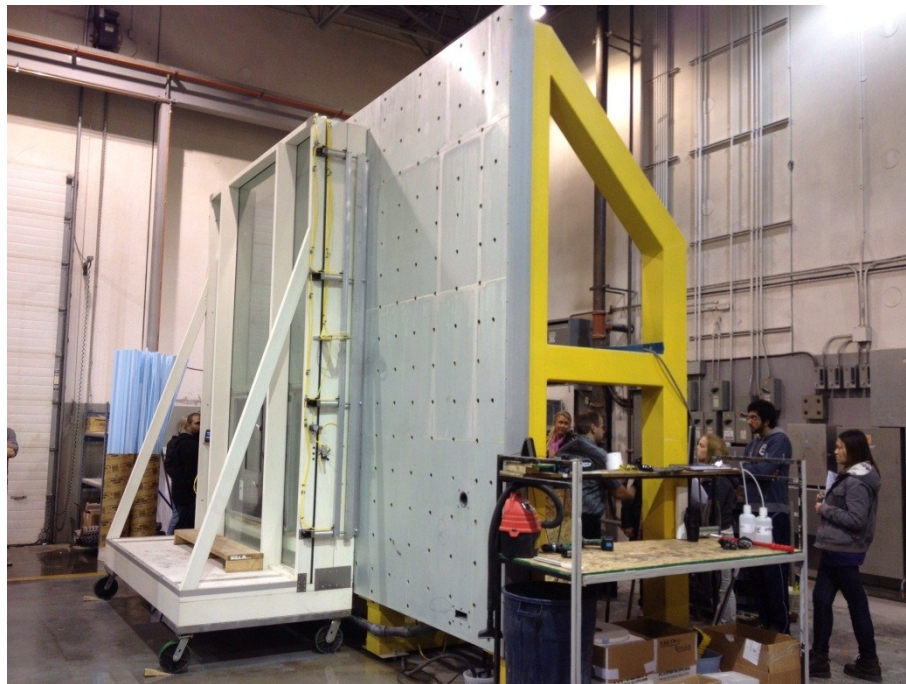


*Figure 21: Test apparatus with movable chamber and window specimen, air and water nozzles, and associated equipment to control air pressure differentials and water spray rate at Cascadia Windows in Langley, BC.*

Test parameters associated with various standards vary and generally involve applying water at a rate of from 120 to 240 L/m<sup>2</sup>·h (mm/h) at pressure differentials of from 137 to 250 Pa, and higher. Refer to Table 2 for a list of test standards and associated test parameters.

Table 2: Summary of water penetration test standards and parameters

Standard	Spray rate (L/m <sup>2</sup> ·min)	Pressure		Source
		Uniform static (Pa)	Cyclic static (Pa)	
AAMA 501.3	3.4	137, 300–600 or 20% of DWP		(American Architectural Manufacturers Association, 1994)
AS/NZS 4284	3	300		(Australian and New Zealand Standards Institution, 1995)
SS 381	4	240 or 30% of DWP1		(Singapore Standard, 1996)
CWCT	3.4	300, 450, 600 or 0.25 of DWP <sup>1</sup>		(Centre for Window and Cladding Technology, 1996)
ASTM 331	3.4	137		(American Society for Testing and Materials, 2000)
BS EN 12155	2.0	150, 300, 450, 600 or >600		(British Standards Institution, 2000)
NT BUILT 421	2.7		200, 400, 600, 800 or 1100	(Nortest Standard, 1993)
AS/NZS 4284	3		150–300, 300-600 or 0.3W-0.6W2	(Australian and New Zealand Standards Institution, 1995)
CSA A 440.1	3.4		137-three cycles	(Canadian Standards Association, 2000)
ASTM E 547	3.4		137-three cycles	(American Society for Testing and Materials, 2000)
<sup>1</sup> DWP – Design wind pressure <sup>2</sup> W – Structural test pressure				

Generally, building codes for particular jurisdictions set out requirements for window performance. In the study region of Metro Vancouver, codes refer to the CSA A440 standard (Canadian Standards Association, 2000) for water penetration resistance<sup>1</sup>. The CSA A440 standard in turn refers to the test methods described in ASTM E331 for static air pressures and ASTM E547 for fluctuating air pressures. The fluctuating air pressures specified in ASTM E547 involve four cycles of pressure application, each cycle consisting of a 5 minute period of with the pressure applied and a 1 minute period

<sup>1</sup> The A440 standard includes companion documents A440.1—a user selection guide to selecting minimum performance levels—and A440.4—an installation guide for new and replacement windows.

without the pressure applied. Water is sprayed continuously over the four cycles of pressure fluctuation.

CSA A-440 also prescribes a method for selecting windows based on *Driving Rain Wind Pressures* (DRWP) corresponding to specific locations. The term DRWP refers to wind pressures that are coincident with the presence of rain for a location at a specified height of 10 m above ground level, for a specific probability of occurrence. The data was prepared by Environment Canada based on climatologically determined wind pressure coincident with the presence of rain for specific locations. The standard also includes a classification system for windows based on their resistance to leakage under specific levels of air pressure differential (Table 3)

*Table 3: CSA A440 classification of rain penetration resistance*

Window rating	Pressure differential (Pa)
B1	150
B2	200
B3	300
B4	400
B5	500
B6	600
B7	700

A procedure for field testing of window installations is also described in ASTM Standard E1105 and a procedure for testing masonry walls is described in ASTM Standard E514. The parameters for E1105 are similar to those of E547. For ASTM E514, the water spray rate is 138 L/m<sup>2</sup>/h and the air pressure differential is 500 Pa, applied for at least 4 hours.

In addition to static and cyclical applications of air pressure differential, some tests call for dynamic applications of air pressure to simulate wind gusts. The test set-ups



(Figure 22) involve a device for rapidly changing the air pressure differential between defined limits. ASTM E2269 includes specifications for testing under dynamic wind pressures between 50% and 150% of a median air pressure at a frequency of 0.5 Hz.

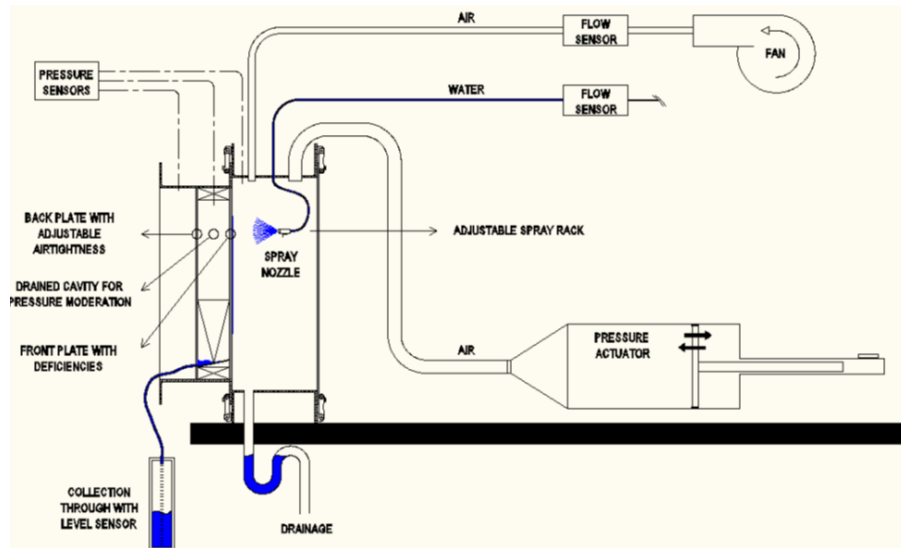


*Figure 22: Window test set-up with a device for rapidly changing the air pressure differential to simulate wind gusts (Lacasse, Moore, & Van Den Bossche, n.d.)*

While current test protocols provide a repeatable and quantifiable basis for the comparison of water penetration resistance of windows, they do not consider local topography and climate effects that impact on the frequency and time of wetness due to rain (RDH Building Engineering, 2002). The evaluation procedures do not, therefore, reflect the risk of water penetration of windows exposed to real weather over long periods.

## 2.5 Correlation of test parameters to field wind-driven rain measurements

Based on a CFD model that he developed in 1994, Choi established theoretical values for Local Intensity Factor (LIF) based on building geometry, location on building, and wind speed (at a reference height of 250 m). Recognizing that the wind-driven rain intensity varies with location on the building façade, Choi divided the windward face of the building, which is 40 m high, 10 m wide, and 10 m deep, into 12 zones defined by

four equally sized horizontal rows and three equally sized vertical columns. Then, using the CFD model, he established the trajectory of the raindrop of a particular diameter,  $r$ , terminating at each corner of each zone. The four trajectories corresponding to a particular zone define an imaginary tube extending upwind to a distance far enough away from the building that the trajectories become nearly parallel and the wind flow field can be considered undisturbed by the influence of the building. A horizontal plane through the tube at this location (i.e. where the wind and rain are undisturbed by the building) defines a cross-sectional area  $h(r)$  for the particular raindrop diameter,  $r$ . The raindrops falling on  $h(r)$  correspond to the raindrops falling on the corresponding zone. The Local Effect Factor for raindrop size  $r$  is then given by the ratio of  $h(r)$  to the area of the zone. By integrating the  $LEF$  for all raindrop diameters using a suitable raindrop size distribution<sup>1</sup>,  $f(r)$ , Choi defined the Local Intensity Factor ( $LIF$ ):

$$LIF_{zone} = \frac{w.d.r. \text{ intensity on zone}}{u.r.i.} = \int LEF(r) \cdot f(r) dr \quad (2.20)$$

where  $w.d.r.$  is the wind-driven rain intensity on the zone (i.e. at a particular location on the building) and  $u.r.i.$  is the undisturbed rainfall intensity. Knowing the  $u.r.i.$ , the  $w.d.r.$  intensity on a particular zone can therefore be computed as the product of the  $LIF$  and the  $u.r.i.$  Finally, using his CFD model and focusing on the zone at the upper corners of the building (termed zone S4) where the  $LIF$  is largest, Choi established a relationship between local intensity factor and wind speed based on a narrow building with height-width-depth dimensions of 40m-10m-10m:

$$LIF_{S4} = 0.025 \cdot V^{1.3} \quad (2.21)$$

---

<sup>1</sup> Choi (1998) used the model by Best (1950) but noted that  $LIF$  values are not sensitive to the drop size distribution model.

where  $V$  is the wind speed in m/s at a height of 250 m.

For considerations of rainwater penetration, Choi chose a 5-minute averaging period to establish the mean wind speed. For many meteorological stations, only hourly mean wind data and gust data is available. In these cases, according to Choi, the 5-minute mean data can be approximated from hourly data as follows:

$$\frac{v(t) - v(3600)}{v(3) - v(3600)} = \left[ \frac{\ln\left(\frac{t}{3600}\right)}{\ln\left(\frac{3}{3600}\right)} \right] \quad (2.22)$$

where

$v(t)$  = the mean wind speed with an averaging period of  $t$  seconds,

$v(3)$  = the gust speed based on an averaging period of 3 seconds, and

$v(3600)$  = the hourly mean speed.

The 5-minute unobstructed rainfall intensity ( $u.r.i.$ ) is obtained from the average hourly value as follows:

$$\frac{u.r.i.(5min)}{u.r.i.(60min)} = \left[ \frac{60}{5} \right]^{0.42} = 2.84 \quad (2.23)$$

The 5-minute wind-driven rain intensity is therefore equal to the product of 2.84, the hourly  $u.r.i.$ , and the Local Intensity Factor ( $LIF$ ):

$$w.d.r.(5min) = 2.84 \cdot u.r.i.(60min) \cdot LIF \quad (2.24)$$

where  $w.d.r.(5min)$  is the 5-minute mean wind-driven rain intensity on the zone,  $u.r.i.(60min)$  is the average hourly uniform rainfall intensity, and  $LIF$  is the local intensity factor for the zone based on the 5-minute mean wind speed at a height of 250m.

Choi applies this approach to a building located in Sydney, Australia to compute 5-minute mean wind-driven rain intensities based on 25 years of hourly wind speed and gust speed data. Sahal and Lacasse (2008) apply the approach to a building in Istanbul,

Turkey based on 9 years of 30-minute mean rainfall intensity and coincident average wind speed. The approach involves selecting the highest wind-driven rain intensity for each period (e.g. for each 5- or 30-minute period) and conducting an extreme distribution analysis. To establish criteria for test pressures, the 5-minute mean wind speed during rain is computed.

Results are presented in a plot of wind-driven rain intensity versus reduced variate (also expressed as a return period), with one point for each year of the study. The points tend to fall on an approximately straight line. To determine conditions for laboratory testing and noting that the provision for water-tightness is a serviceability requirement, Choi used a 10-year return period in his analysis. The water spray rate is based directly on the *w.d.r.* intensity (mm/h) corresponding to a 10-year return period:

$$\text{Test spray rate} = w.d.r.(5\text{min}) \quad (2.25)$$

where *w.d.r.*(5min) is the 5-minute mean wind speed corresponding to a 10-year return period.

The air pressure differential is computed as follows based on the mean 5-minute wind speed corresponding to a 10-year return:

$$\text{Test pressure} = C_p \cdot \frac{1}{2} \cdot \rho \cdot V_{5\text{-minute during rain}}^2 \quad (2.26)$$

where  $\rho$  is the air density and  $C_p$  is the pressure coefficient, the latter taken equal to 1 to represent the critical pressure.

## 2.6 Summary of findings

Wind and rain in combination cause wind-driven rain loads on vertical surfaces of buildings. The understanding of wind-driven rain has been significantly influenced by the concept driving rain index—the product of horizontal rainfall intensity and wind speed.

Vancouver has weather characteristics peculiar to its temperate rainforest, marine, and mountainous surroundings that influence the wind and rain patterns in the region. Its relative proximity to the Aleutian Islands of Alaska, which is the origin of intense low pressure systems that persistently settle off shore of Canada's west coast, is also a significant influence. Behaviours are complicated by topographical influences, building form, and turbulence. Building codes specify standards for window performance under wind-driven rain exposure and typically refer to CSA A440—a standard for rain penetration resistance of windows—which in turn refers to other standards that provide specific test protocols. The tests results provide a useful basis of comparison for window performance in general but do not represent loading under real weather conditions and can't be used to predict the risk of failure of windows exposed to long-term, real weather conditions. This may be particularly true in coastal British Columbia's climate, where frequency of rain event and time of wetness may be critical factors. Some research has been done to link common test parameters to actual measurements of wind-driven rain on buildings in Sydney Australia and in Turkey, but no such studies have been undertaken in coastal British Columbia's unique climate. A study of actual wind-driven rain measured on the walls of buildings in Metro Vancouver, which is the centre of population in coastal British Columbia, will help to clarify the appropriateness of current parameters for window testing and may lead to suggestions for improvements and further research.

## CHAPTER 3: METHOD

With the aim of this study being to provide realistic estimates of wind-driven rain on buildings that may help to improve testing methods for windows, the method involves collecting measurements of actual wind-driven rain and then linking the results to specific parameters for testing windows. The method of linking the measured wind-driven rain with parameters for testing is based in part on the approach by Choi (1994; 1998). At least 25 years of historical wind, rain, and wind-driven rain data are ideally required at a site to conduct the analysis to determine the water spray rate and air pressure differential corresponding to a specific return period. Historical data collected at the airport under free field conditions are available but do not include measurements of wind-driven rain impinged on a building surface and do not represent realistic exposure conditions for urban environments. The approach for this study is to take *short-term* measurements of wind-driven rain on several buildings in the Metro Vancouver region using wind-driven rain gauges mounted on the walls of the buildings, and then link the data to 25 years of *historical data* measured at the airport. The linkage is established through analysis of the measured catch ratio—the ratio of wind-driven rain measured by a vertical plate gauge mounted on the wall of a building to the horizontal rainfall intensity measured by standard horizontal rain gauge mounted above the roof of the building. The sites are chosen to represent a range of building geometry and topographical and urban surroundings to establish realistic catch ratios for buildings in the unique climate of Metro Vancouver. The locations of individual wind-driven rain gauges on the buildings are selected to capture a range of expected wetting, from the upper corners and top edges of walls—where the most intense wind-driven rain is expected—to locations where little

or no wind-driven rain is expected. Analysis of this data leads to a calculation of water spray rate and air pressure differential corresponding to various return periods for several categories of building form.

### 3.1 Gathering and analysis of short-term building site data

This part of the research involves taking measurements of wind-driven rain at building sites in Metro Vancouver during the winter season, and then establishing the relationship between catch ratio and wind speed. Beginning with a description of the buildings selected for this study, this section includes details of the method of instrumentation and data acquisition employed in the study and concludes with the methodology used to establish the relationship between catch ratio and wind speed.

#### 3.1.1 *Building selection and description*

A total of thirty five buildings that are part of the housing stock of the BC Housing Management Commission (BCHMC) were originally considered for study. Of these, seven buildings were selected and were fitted with instrumentation and data acquisition systems to measure wind speed and direction, horizontal rainfall intensity, and wind-driven rain intensities at up to eight locations on each building<sup>1</sup>. A preliminary analysis of the data has been performed and reported (Ge & Krpan, 2007). Based on results from the preliminary analysis and objectives for the current study, three of the original seven buildings were selected for further study. The selections represent a range of location, geometry and massing and are amongst those thought to have the most reliable data of the seven originally considered. The three buildings are identified by their street names: *Keefe*, *Kingsway*, and *Wallace*. All of the buildings are multi-family

---

<sup>1</sup> Collection of the building site data was facilitated through the Building Science Centre of Excellence (BSCE) at the British Columbia Institute of Technology (BCIT).

residential occupancies. Locations of the buildings are shown in Figure 23, and photographs of the buildings are provided in Figure 24. Details concerning building geometry are provided in the Appendix.

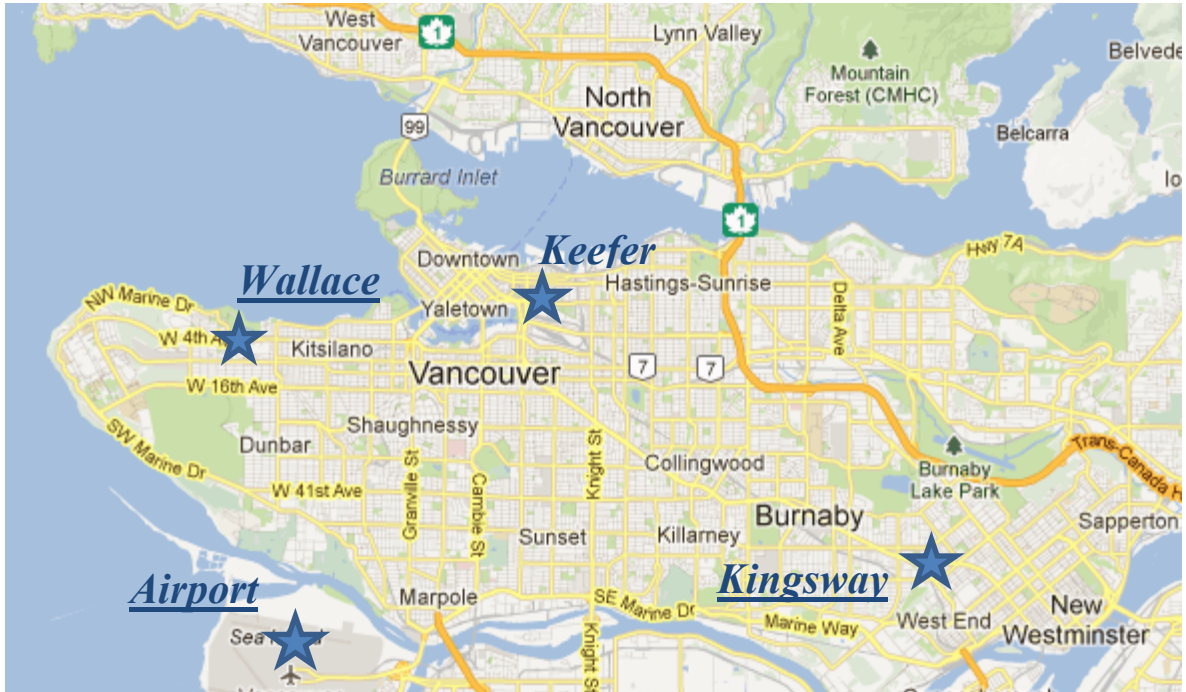


*Figure 23: Map showing location of Keefe, Kingsway and Wallace building sites as well as the Vancouver International Airport.*

Keefe is a high-rise building located east of the downtown core of Vancouver outside the zone of high-rise residential and commercial towers that dominate the downtown landscape. Most of the buildings in its immediate surroundings are low rise buildings. It is within one kilometre of the Burrard Inlet waterfront, which lies to the north. The low and flat areas to the immediate south-east of Keefe are bounded by hills. The building has a 900 mm roof overhang. Kingsway is also a high-rise building located on a high point of land about 15 km inland of the waterfront within a cluster of surrounding midrise buildings in the immediate vicinity and with low-rise buildings beyond. Kingsway does not have a roof overhang. Wallace is a low-rise building—varying between three and four stories—with broad profile. With Jericho beach lying to



the immediate north, Wallace is located nearest to the waterfront of any of the three buildings considered in the study. It is also adjacent to a park with trees at least equal in height to the building. The elevation rises beyond the area to the immediate south of Wallace toward the neighborhoods of Kitsilano and Dunbar.

### *3.1.2 On-site measurement of wind and horizontal rainfall*

The wind speed and direction and the horizontal rainfall intensity are measured at each building site. The wind speed and direction are measured with a propeller anemometer and wind vane mounted on a mast at a height of 3 m above the roof surface. The mast is located near the centre of the roof. The measuring range is 0 to 60 m/s for wind speed and 0 to 355° for wind direction. The horizontal rainfall is measured by a tipping bucket rain gauge placed on the roof, located as close to the centre as possible to minimize wind disturbance. Two types of horizontal rain gauge are used. Although they have different catchment areas, one bucket tip for either gauge corresponds to 0.1 mm of accumulation measured on a horizontal plane. Each bucket tip produces an electronic pulse that is recorded in 5-minute bins (i.e. the number of bucket tips in each 5-minute period is recorded).



*Keefer*



*Kingsway*



*Wallace*

*Figure 24: Photographs of the three buildings (from top): Keefer, a high-rise building with roof overhang located east of the downtown core; Kingsway, a high-rise building located inland at an exposed location; and Wallace, a low and wide building located near waterfront*

### 3.1.3 *Measurement of wind-driven rain impinged on walls*

The amount of wind-driven rain impinged on the walls of the buildings is measured using customized driving rain gauges. To help minimize measurement errors, a variety of materials and geometries were explored before adopting the final wind-driven rain gauge for this study. In total five materials are considered for the collection surface, including glass, polymethyl-methacrylate (PMMA, acrylic), aluminium, stainless steel, and polished stainless steel. To identify the material most likely to minimize adhesion error, laboratory tests are conducted to measure the adhesion water for each material. A rectangular plate rain gauge measuring 254 mm by 304.8 mm is fabricated from each of the materials (except the polished stainless steel). The polished stainless steel is fabricated to dimensions of 228.6 mm by 228.6 mm. Each plate is subjected to 10 spray cycles using a spray bottle with adjustable nozzle. The spray nozzle is maintained at a constant distance from the specimen with approximately consistent spray speed and droplet sizes. In each cycle, the sample is sprayed at four spots to cover the entire area until a significant amount of runoff occurs. The plate is then weighed and the mass of the adhesion water is calculated. Tap water is used for these experiments. The absolute measurement errors due to adhesion for each material are listed in Table 4.

While glass has the least adhesion water of the materials tested, it is relatively heavy and difficult to fabricate and install. The performance of polished stainless steel and acrylic are similar. Electro-plated stainless steel (14-gauge) was chosen as the material for the driving rain gauge because of its durability and adhesion characteristics. A diamond shaped collector with dimensions of 228.6 mm by 228.6 mm was chosen, as shown in Figure 25 and Figure 26. The collector edge projects 25.4 mm out from the wall

surface at an angle of 45° away from the collector surface to direct runoff rainwater away from the gauge. The projection of the collector edge is chosen to minimize disturbance of the wind flow field and raindrop trajectories while still effectively deflecting runoff water from above. To minimize adhesion water, the connection tube from the collector to the tipping bucket is made as short as possible (about 100 mm). The tipping bucket chosen for the driving rain gauge has a resolution of 2 g per tip, which is equivalent to 0.0383 mm of accumulation on a horizontal plane for the 228.6 x 228.6 mm collection area.

*Table 4: Adhesion water on vertically aligned plates of varying material*

	Glass	PMMA	Aluminum	Stainless steel	Polished stainless steel
Plate width (mm)	254.0	254.0	254.0	254.0	228.6
Plat height (mm)	304.8	304.8	304.8	304.8	228.6
Adhesion water (mm or L/m <sup>2</sup> )	0.047	0.066	0.083	0.081	0.074

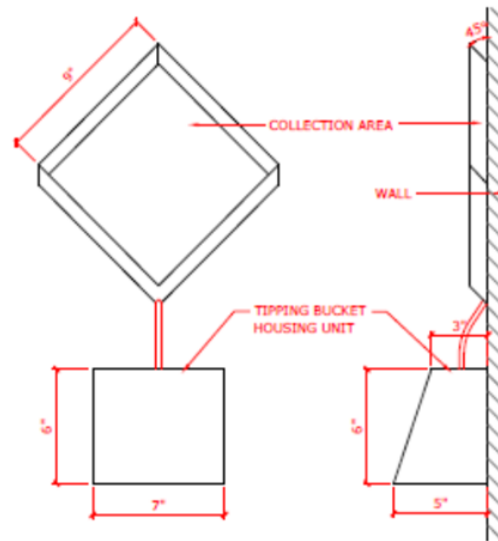


*Figure 25: Diagram of the wind-driven rain gauge showing dimensions of the diamond-shaped collection area and housing unit for the tipping bucket mechanism (Ge & Krpan, 2009)*



*Figure 26: Photograph of a prototype of the wind-driven rain gauge deployed on a campus building*




Qualitative observations have led to an awareness of typical wetting patterns on buildings, generally consisting of concentrations at upper corners and top edges, as shown in Figure 27 for a high-rise building. The wind-driven rain gauges for this study are installed in locations on the building to capture an expected range of wetting conditions, from maximums at the upper corners and top edges of buildings to minimums at sheltered or mid-field locations.



*Figure 27: Sequence of photographs showing the characteristic wetting pattern of a wall of a high rise building in Vancouver with south-east exposure*

Eight rain gauges are installed on the Kingsway building and six gauges are installed on the Keefer and Wallace buildings. Most of the gauges are located on the east- and south-facing walls where exposure to wind-driven rain is expected to be highest. A summary description of each building with the general location of the wind-driven rain gauges on various wall orientations is provided in Table 5. Specific information on the location of wind-driven rain gauges for each building is available in the Appendix.

*Table 5: Summary description of the three subject buildings including form and overhang geometry, location description, and general arrangement of wind-driven rain gauges*

Name	Form	Overhang geometry	Photograph	Building location	Gauge locations			
					N	E	S	W
<b>Keefer</b>	High-rise with moderate aspect ratio	900 mm overhang		Vancouver with wind mast on 2-storey mechanical penthouse and rain gauge on main roof	-	4	2	-
<b>Kingsway</b>	High-rise, with tall, narrow aspect ratio	No overhang		Burnaby with mast on 2-storey mechanical penthouse	1	5	1	1
<b>Wallace</b>	3-storey & 4-storey low-rise with broad aspect ratio	No overhang		Vancouver (near Jericho beach) with mast on roof	1	3	1	1

### 3.1.4 Catch ratio and wind speed

Data measured at the building sites is used to establish the relationship between wind-speed and catch ratio at specific locations on real buildings in Metro Vancouver’s climate. The catch ratio is also influenced by wind direction and horizontal rainfall intensity. For this study, the catch ratio is evaluated for wind directions normal to the wall surface (i.e. the wind direction is parallel to a normal drawn perpendicular to the wall surface). Blocken (2004) has explored the relationships between catch ratio and horizontal rainfall intensity and wind speed using a Computational Fluid Dynamics (CFD) approach. Results for a high-rise building with dimensions of 20x20x80 m and a low-rise building with dimensions of 10x10x10 m are shown in Figure 28 in the form of three dimensional plots. In each case, the catch ratio is predicted based on a location on

the wall at the top corner of the building and for a wind direction normal to the wall surface. As shown, the influence of rainfall intensity is negligible relative to the influence of wind speed, except for very low rainfall intensities where the influence of rainfall intensity becomes slightly more significant. At low horizontal rainfall intensities, less than about 3 mm/h, Blocken's analysis predicts a slight increase in catch ratio for a low-rise building and a decrease in catch-ratio for a high-rise building. For this study, in which the catch ratio is characterized using measured data rather than a CFD model, the influence of rainfall intensity has been neglected and the catch ratio for a particular location and wind direction is assumed to depend only on wind speed.

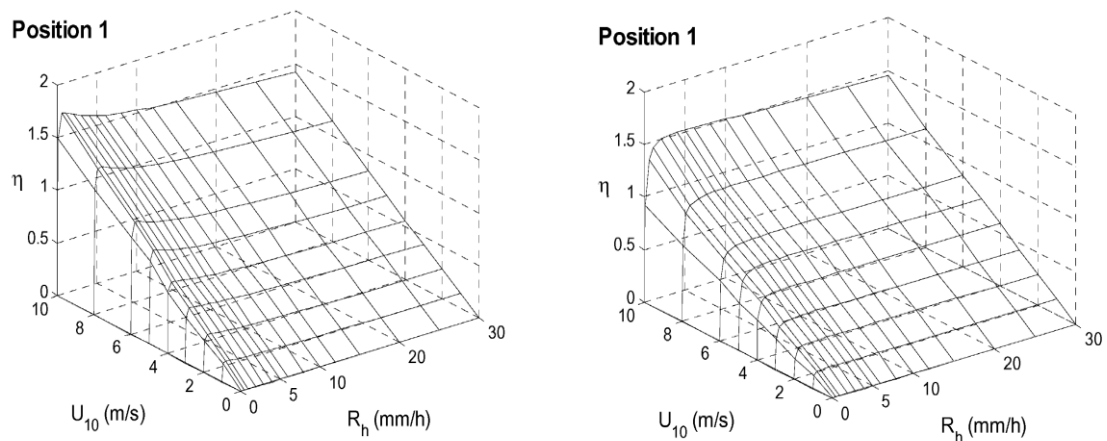


Figure 28: Three dimensional plots showing variation of catch ratio with wind speed and horizontal rainfall intensity for the top corner of a low-rise building (left) and high-rise building (Blocken, 2004)

A typical scatter plot of measured catch ratio and corresponding wind speed obtained from this study is shown in Figure 29. The data can be fitted by quantile regression to a curve of the form

$$\eta = a \cdot U^b \tag{3-1}$$

where

$\eta$  is the catch ratio,



$U$  is the wind speed, and

$a$  and  $b$  are constants chosen to fit the measured data.

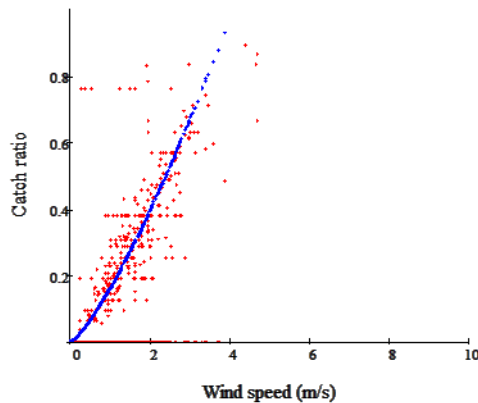


*Figure 29: Typical scatter plot of measured catch ratio versus wind speed with fitted curve*

An expression for catch ratio is determined in this manner for each building site and each wind-driven rain gauge location. The results are then used, as described in Section 3.2, to compute the expected wind-driven rain intensity corresponding to various return periods at the airport.

### 3.2 Analysis of historical airport data

The wind-driven rain measurements for this study are collected over a relatively short period of time, about four months, which is too short a period to be statistically relevant for projecting long term (10- and 20-year) return periods for water spray rate. The catch ratios measured at each of the building sites are therefore linked to historical wind and rain data collected at the airport. The purpose of this part of the analysis is to establish return periods corresponding to specific wind speeds and wind-driven rain intensities at the airport, which are in turn used to compute the corresponding test pressure and water spray rate.

Based on the wind speed and horizontal rainfall intensity measured at the airport over a 25-year period, the wind-driven rain that would be expected on the surface of a building under these conditions is computed using the expression for catch ratio as a function of wind speed derived based on measured data at the building sites. An extreme distribution analysis is then conducted to determine the relationship between wind-driven rain intensity and return period. Details of the procedure are described in the analysis given in Section 4.2.3.

### 3.3 Calculation of air pressure differential and water spray rate

The final step in the analysis is to compute the water spray rate and air pressure differential. The test pressure is taken as the product of the pressure coefficient at the location of a specific wind-driven rain gauge and the theoretical stagnation pressure at that location, as follows:

$$\text{Test pressure} = C_p \cdot \frac{1}{2} \cdot \rho \cdot V^2 \quad (3-2)$$

where

$C_p$  is the pressure coefficient,

$\rho$  is the density of air, and

$V$  is the wind speed.

The water spray rate is taken equal to the wind-driven rain intensity, which is computed as the product of the horizontal rainfall intensity measured at the airport for a specific return period and the catch ratio, where the catch ratio is a function of wind speed as determined from analysis of the building site data, as follows:

$$\text{Water spray rate} = R_{wdr} = R_h \cdot \eta = R_h \cdot a \cdot V^b \quad (3-3)$$

where

$R_{wdr}$  is the computed wind-driven rain intensity,

$R_h$  is the horizontal rainfall intensity,

$\eta$  is the computed catch ratio,

$V$  is the wind speed, and

$a$  and  $b$  are constants determined from the building site analysis.

Details of the procedures to compute air pressure differential and water spray rate are given in the analysis described in Section 4.3.

## CHAPTER 4: ANALYSIS

This chapter presents the analysis in three sections corresponding to the major steps in the process: *4.1 Analysis of short-term building site data*, *4.2 Analysis of historical airport data*, and *4.3 Calculation of test conditions*. The short-term building site data analysis begins with preprocessing of the raw data, including filtering to exclude unwanted or suspect data. For each wind-driven rain gauge on each building (20 wind-driven rain gauges in total), the catch ratio is then computed and plotted against wind speed. Based on the resulting scatter plot, an expression for catch ratio as a function of wind speed is developed. The historical airport data analysis includes preprocessing of the data, which was collected by and obtained from Environment Canada. Based on wind speeds and rainfall intensities measured at the airport, the wind-driven rain intensity is computed using the expression for catch ratio derived from the building site data, thus linking the two sets of data. An extreme distribution analysis of the results leads to expressions for wind speed and wind-driven rain intensity as a function of return period. In the final step, calculations for test conditions based on return periods of 10- and 20-years, including water spray rate and air pressure differential, are presented and compared to current standards and other published data.

### 4.1 Analysis of short-term building site data

#### *4.1.1 Description of raw building site data*

The raw data set for each building site comprises all of the 5-minute mean data collected from November 11, 2007 at 00:05 hours to February 29, 2008 at 24:00 hours<sup>1</sup>. Measurements for each five minute period ending are recorded. That is, the first data

---

<sup>1</sup> Some preprocessing of the data was conducted and reported as part of an earlier study (Ge & Krpan, 2009).

recorded are on November 11, 2007 at 00:05 hours and correspond to the 5-minute period from 00:00 to 00:05 hours. For this and each subsequent 5-minute period ending, the wind speed, wind direction, number of horizontal rain gauge bucket tips, and number of wind-driven rain gauge bucket tips for each gauge location are recorded.

One anemometer, one horizontal rain gauge, and from six to eight wind-driven rain gauges are deployed at each site<sup>1</sup>. The wind speed is recorded in m/s, and the wind direction is recorded in degrees measured clockwise from north. Each tip of a horizontal rain gauge bucket corresponds to 0.1 mm of accumulation, and each tip of a wind-driven rain gauge bucket corresponds to the equivalent of 0.038 mm of accumulation on a horizontal plane. An identifying index number for each wind-driven rain gauge at each site is shown in Table 6, along with the orientation of the wall at the location of the gauge. The wall orientation is measured clockwise from north to the normal to the wall at the location where the particular gauge is mounted.

*Table 6: Name and corresponding wall orientation in degrees for each wind-driven rain gauge at each building site*

Gauge Index	Building Site					
	Kefer		Kingsway		Wallace	
	Name	Wall	Name	Wall	Name	Wall
0	East-mid	90	East-4th	90	East Balcony	90
1	East-top	90	East-north-top	90	East Top	90
2	South-tile	180	North	0	East Bottom	90
3	South-concrete	180	West	270	North	0
4	East-bottom	90	E Brick top	90	West	270
5	East-North	0	South	180	Yard	0
6	n/a	n/a	E Brick 2nd	90	n/a	n/a
7	n/a	n/a	E Brick 3rd	90	n/a	n/a

<sup>1</sup> Six wind-driven rain gauges are deployed at the Kefer and Wallace sites and eight such gauges are deployed at the Kingsway site, as described in Section 3.1.3.

#### *4.1.2 Preprocessing of building site data*

Wind speeds and directions are filtered for low wind speeds during the measuring period (less than 0.3 m/s). The data is found to include a delay between tips of the horizontal bucket and tips of the wind-driven rain buckets, which produces erroneous results when parameters such as catch ratio are computed. The data are therefore transformed from a 5-minute averaging period to an hourly averaging period. Mean values for wind speed and direction are computed over each one hour averaging period. The number of bucket tips over each one hour averaging period is summed. The data set is truncated to result in an even number of hourly averaging periods. The total number of hourly averaging periods for each site is 2664 (which corresponds to 2663 indices numbered from 0).

The resulting hourly wind-driven rain gauge bucket tips are filtered for averaging periods with no co-occurring horizontal rain gauge bucket tips (i.e. wind-driven rain measurements are discarded when there is no recorded horizontal rain over the same period). Wind-driven rain bucket tips are also filtered for measuring periods with no co-occurring wind directed toward the wall over the averaging period. The wind direction is considered to be toward the wall when its direction is within 22.5 degrees to the normal to the wall.

The horizontal rainfall and wind-driven rain intensities for each averaging period (mm/h) are computed by multiplying the number of horizontal bucket tips by 0.1 and the number of wind-driven rain bucket tips by 0.038. Dry and calm measuring periods are then filtered to leave only wet and windy periods (i.e. periods for which horizontal rain and wind speed are both greater than zero). The percentage of the total number

measurement periods that have coincident non-zero values of wind speed and rainfall intensity (after filtering) is 23%, 55%, and 22% for Keefer, Kingsway and Wallace, respectively.

#### 4.1.3 Overview of processed building site data

This section presents analysis of the temporal and frequency distributions of wind speed and direction and the temporal distribution of horizontal rainfall and wind-driven rain intensities. The purpose of this analysis is to further describe the data set and to ensure that the preprocessing steps adequately exclude unwanted information, such as instances when the rain gauges were being cleaned or had malfunctioned.

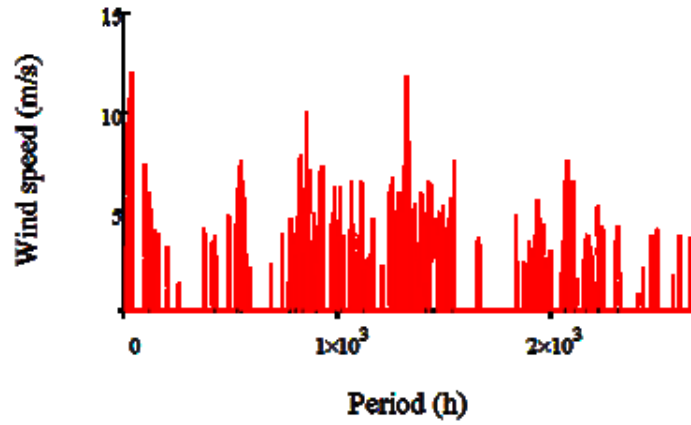
##### 4.1.3.1 Wind speed and direction

The overall average and maximum wind speeds measured over the 2664 one hour averaging periods (111 days in total) for each building site are listed in Table 8. The highest overall wind speed is measured at Kingsway at 16.7 m/s. The highest average wind speed of 4.0 m/s is measured at Keefer. Wallace generally had the lightest wind speeds of the three sites, with an average of 1.4 m/s and a maximum of 4.7 m/s.

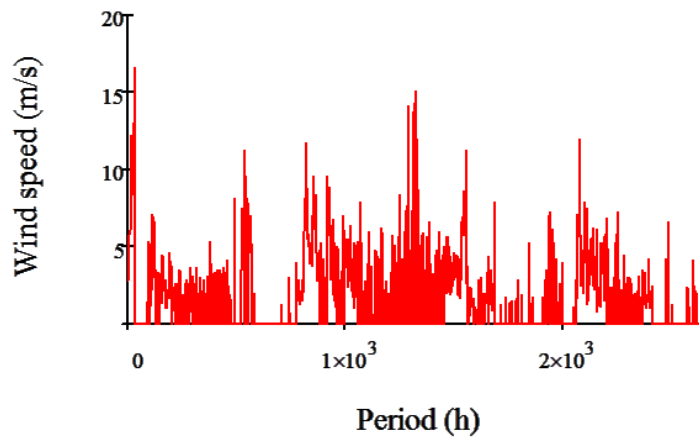
*Table 7: Average hourly and maximum wind speed for each building site*

	Wind speed (m/s)	
	Average hourly	Maximum
Keefer	4.0	12.0
Kingsway	3.6	<b>16.7</b>
Wallace	1.4	4.7

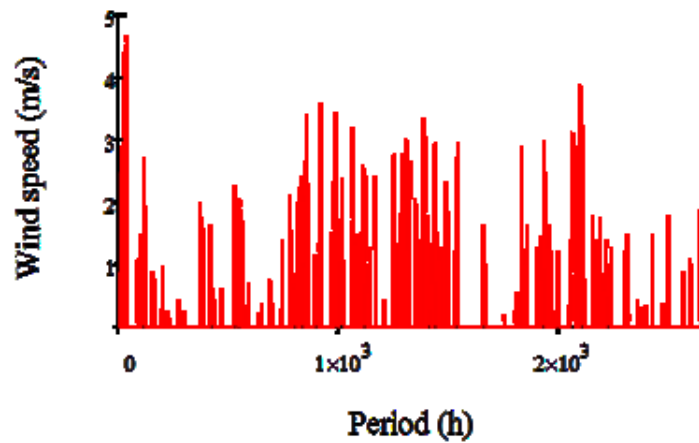
The temporal distribution of wind speed is shown in Figure 30 for each building site. The distributions at the three sites show similar patterns of high wind over the measuring period, each beginning with high wind speeds at the start of the measuring period followed by three peaks through the remainder of the measuring period.



*Keeper*



*Kingsway*



*Wallace*

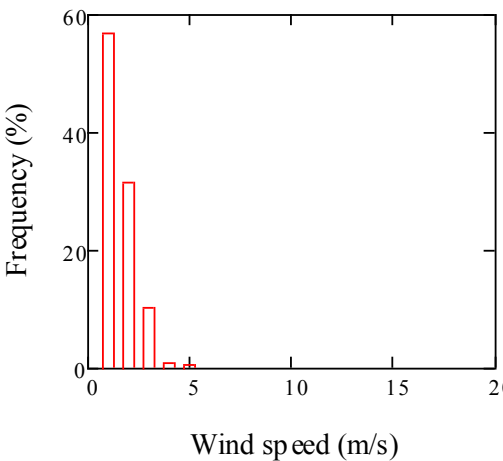
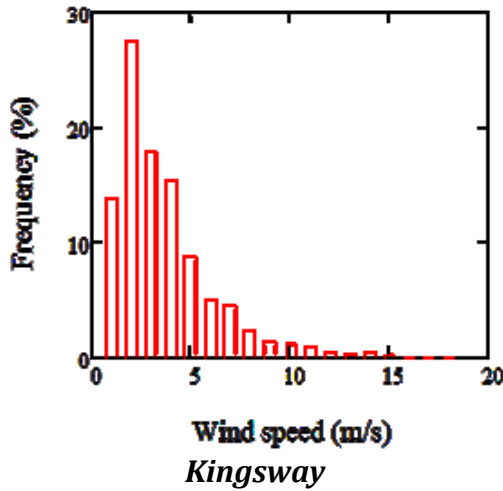
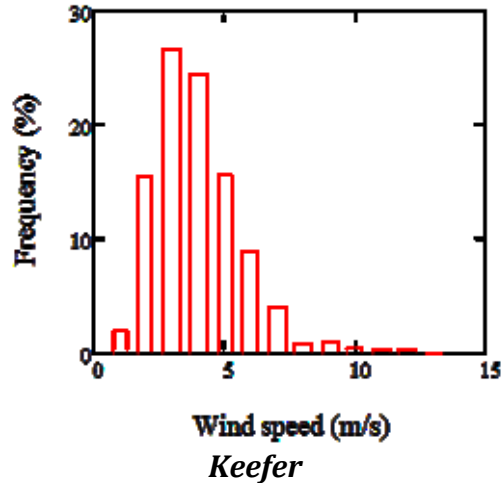
Figure 30: Temporal distribution of wind speed measured at the centre of the roof of the building and 10 metres above its surface



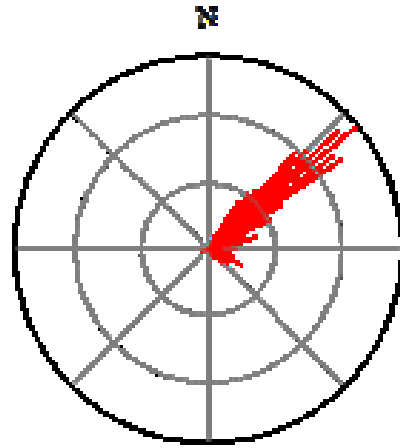
Figure 31 shows the frequency distribution of wind speed based on 1 m/s bin intervals. Kingsway has the broadest distribution, with measured wind speeds from less than 0.5 m/s through to 18 m/s, and Wallace has the narrowest distribution, with measured speeds to only 5 m/s.

Figure 32 shows the frequency distribution of wind direction for each site based on a 128 point rose. The winds at Keefer are predominantly from the north-east, and those for Kingsway and Wallace are predominantly from the east. Kingsway shows a narrow concentration in the distribution from the east and a relatively even distribution among other compass points. Wallace, by contrast, shows a scattered distribution between north-east and south-east, with relatively little of the distribution among other compass points.

The results are generally consistent with those reported in the literature, though the wind direction measured at Keefer differs somewhat from results reported in the literature (Section 2.1.4). Based on the literature, the Keefer site could be expected to show a strong easterly orientation to the wind direction, like the other sites, but measurements for the current study show a pronounced north-east orientation. The difference could be related to the complex nature of topographical influences in the region. The average wind speeds over the measuring period are generally less than expected based on the mean annual levels reported in the literature.

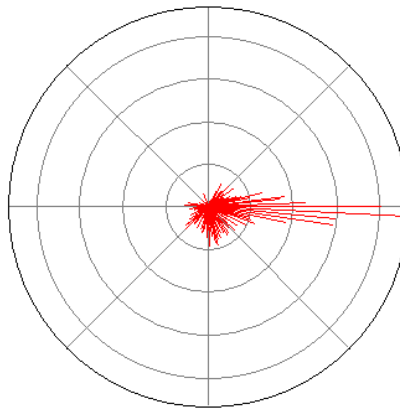


**Wallace**  
 Figure 31: Frequency distribution of wind speed corresponding to 1 m/s bin intervals



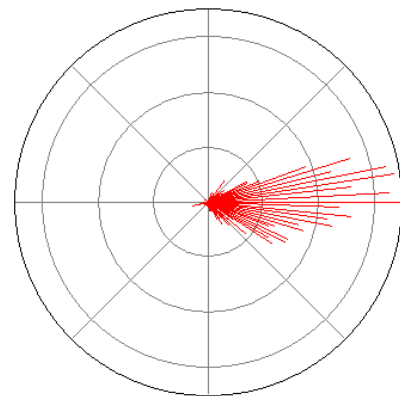
**Kefer**

N



**Kingsway**

N



**Wallace**

*Figure 32: Frequency distribution of wind direction (128-point rose) measured from north at top*

#### 4.1.3.2 Horizontal rainfall intensity

The average and maximum horizontal rainfall intensity for each building site are summarized in Table 8. The highest maximum intensity of 15.2 mm/h of accumulation on a horizontal plane is measured at Kingsway. Keefer and Wallace show maximums of about 6 mm/h and averages of about 1 mm/h.

Table 8: Average and maximum horizontal rainfall intensity for each building site

	Horizontal rainfall intensity (mm/h)	
	Average	Maximum
Keefer	1.0	6.2
Kingsway	0.3	<b>15.2</b>
Wallace	0.9	6.0

The temporal distribution of horizontal rainfall intensity is shown in Figure 33. The distribution of measured rainfall intensity varies widely between the sites. Kingsway is characterized by extremes of high and low rainfall intensities; Keefer and Wallace are more consistent but show little correlation with one another.

#### 4.1.3.3 Wind-driven rain intensity

The average and the maximum wind-driven rain intensity measured at each gauge at each building site are listed in Table 9.

Table 9: Average and maximum wind-driven rain intensities (mm/h) for each gauge at each building site

Building site		Wind-driven rain gauge index number							
		0	1	2	3	4	5	6	7
Keefer	Average	0.21	0.22	0.27	0.30	0.06	0.13	n/a	n/a
	Maximum	2.8	<b>3.0</b>	1.0	1.3	0.2	0.9	n/a	n/a
Kingsway	Average	0.10	0.24	0.15	0.16	0.30	0.20	0.24	0.13
	Maximum	0.8	2.7	0.4	0.4	<b>3.6</b>	1.4	3.1	1.4
Wallace	Average	0.34	0.22	0.14	0.05	0.16	0.0	n/a	n/a
	Maximum	<b>3.0</b>	1.8	0.9	0.1	0.4	0.0	n/a	n/a

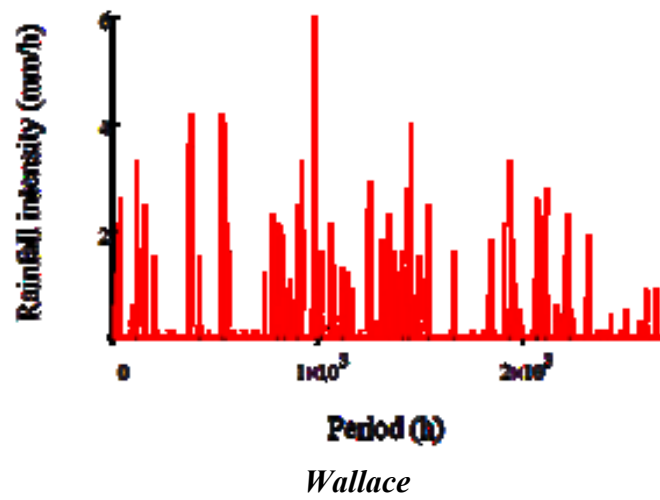
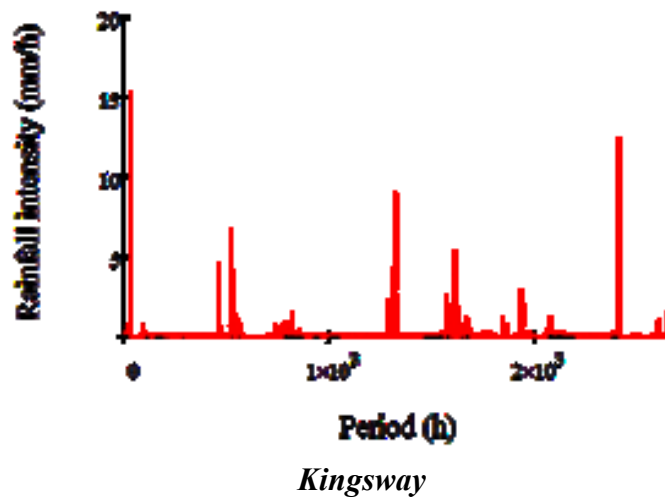
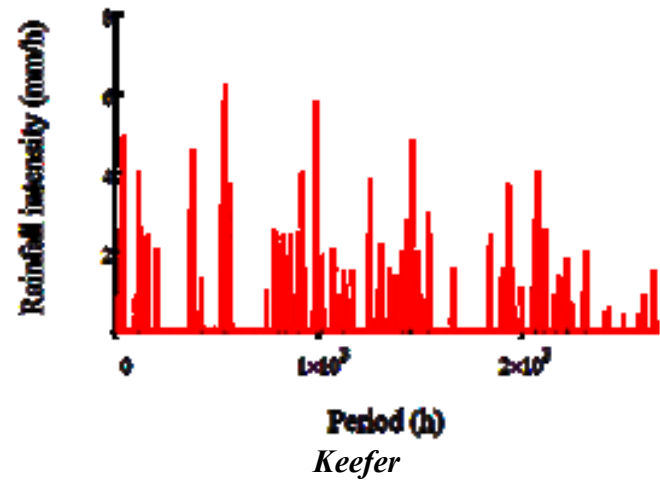
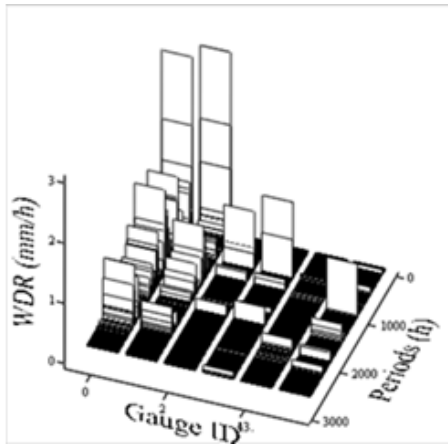
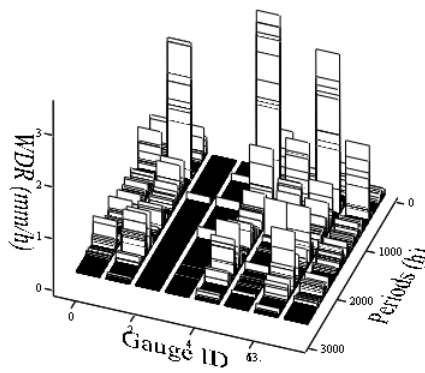


Figure 33: Temporal distribution of horizontal rainfall intensity

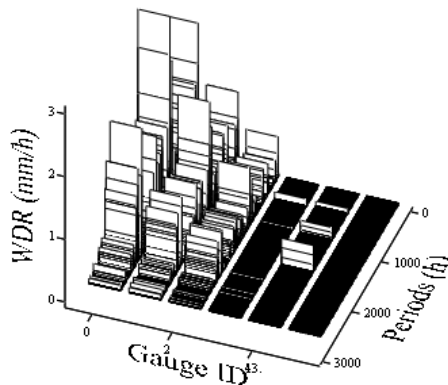
The overall maximum wind-driven rain intensity of 3.6 mm/h is measured at Kingsway at gauge 4 (E Brick top). The maximums at Keefer and Wallace are both 3.0 mm/h measured at gauges 1 (East-top) and 0 (East Balcony) respectively. The maximum wind-driven rain intensities in each case are measured on east-facing walls. The maximums at Kingsway and Keefer are measured at upper corners; the maximum at Wallace is measured at a balcony edge. The gauges placed at Wallace show the broadest range of measured wind-driven rain intensity, from zero in the case of gauge 5 (Yard) to 0.34 mm/h for gauge 0 (East Balcony). Gauge 5 (Yard) at Wallace is located in a sheltered courtyard, and so the result (i.e. no recorded wind-driven rain after filtering) is not unreasonable. Gauge 0 (East Balcony) at Wallace, which has the highest average wind-driven rain intensity, is mounted on an east-facing balcony edge. The highest average wind-driven rain intensities measured at Keefer and Kingsway are both 0.3 mm/h, at gauges 3 (South-concrete) and 4 (E Brick top) respectively. The locations of highest average wind-driven rain intensity are a south-facing top corner in the case of Keefer and an east-facing top corner in the case of Kingsway. In general, the maximum wind-driven rain intensities and highest averages (over the measurement period) tend to occur on east-facing walls and, except for the low-rise Wallace building, at the upper corners. The east-facing wall at Keefer is protected by a large roof overhang of about 1 metre while the south-facing wall is more exposed and therefore receives the greater wind-driven rain load. Given that the prevailing wind direction for Keefer is from the north-east, this result demonstrates the significant influence of roof overhang on reducing the wind-driven rain load. The temporal distribution of wind-driven rain intensity measured at each gauge at each building site is shown in Figure 34.



*Keefe*



*Kingsway*



*Wallace*

Figure 34: Temporal distribution of wind-driven rain (WDR) intensity for each gauge at each building site for the period of record

The highest recorded wind-driven rain intensities occur at the start of the period of record, which is also when the highest wind speeds are observed at each site. The results show the highest consistent wind-driven rain intensities recorded at gauges 0 (East-mid) and 1 (East-top) for Keefer; gauges 1 (East-4<sup>th</sup>), 4 (E Brick top), and 6 (E Brick 2<sup>nd</sup>) for Kingsway; and gauges 0 (East Balcony), 1 (East Top), and 2 for Wallace (East Bottom).

#### 4.1.4 Catch ratio computed from building site data

The catch ratio is computed for each hourly period for each wind-driven rain gauge at each of the building sites:

$$\eta = \frac{R_{wdr}}{R_h} \quad (4-1)$$

where

$\eta$  is the catch ratio,

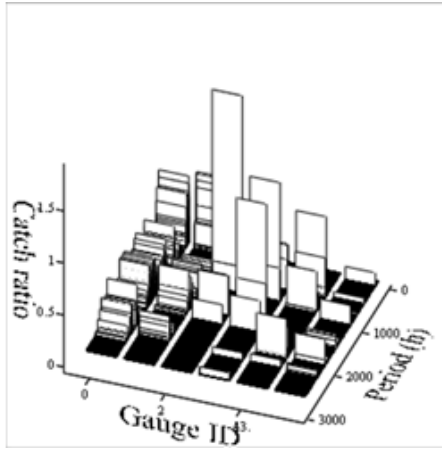
$R_{wdr}$  is the wind-driven rain intensity measured at the wall, and

$R_h$  is the horizontal rainfall intensity measured above the roof.

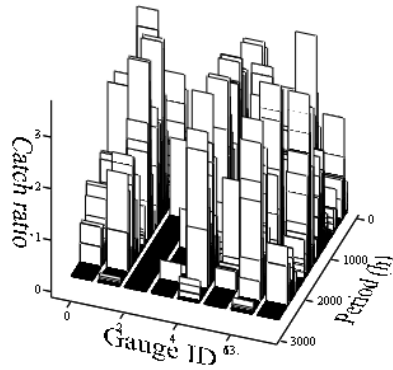
The temporal distribution of catch ratio for each building site and gauge location is shown in Figure 35. The catch ratios computed for Kingsway are consistently high for all gauges throughout the period of record. For one of the gauges at Wallace located in a sheltered courtyard, the catch ratio is zero (after filtering). At Wallace, only gauge 0 (East Balcony), 1 (East Top), and 2 (East Bottom) show significant catches throughout the period.

The relationship between catch ratio and wind speed is established for one wind-driven gauge location at each building site. The chosen location has consistently high catch ratios throughout the period of record in each case: gauge 2 (South-tile) for Keefer, gauge 4 (E Brick top) for Kingsway, and gauge 1 (East Balcony) for Wallace.

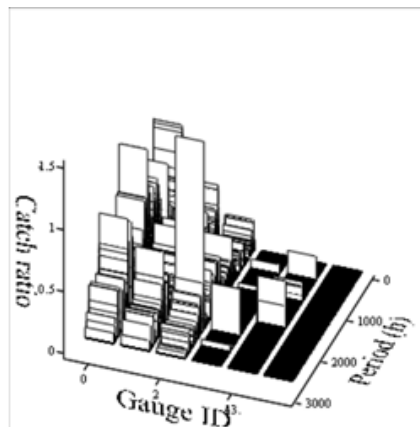




*Keefer*



*Kingsway*



*Wallace*

*Figure 35: Temporal distribution of catch ratio for each gauge at each building site for the period of record*

The gauges at Kingsway and Wallace are east-facing and located near the top of their respective buildings. The gauge at Keefer is south-facing at a location where the overhang is less. A scatter plot with catch ratio as a function of wind speed is shown in Figure 36 for each building along with a curve fitted to the mean data. These expressions for catch ratio are applied in the next section to determine wind-driven rain intensities based on historical airport data. The fit for Wallace and Keefer are reasonably good; the fit for Kingsway is poor.

#### *4.1.5 Summary of findings from building site analysis*

Wind-driven rain is significantly influenced by building geometry, particularly roof overhang. In this study, for example, the catch ratio for a low-rise building without overhang was higher than observed for a high-rise building with roof overhang. The effect of the overhang is to reduce the intensity of wind-driven rain loads at the location where they would otherwise be highest. Perhaps counter-intuitively, low-rise buildings may have higher catch ratios than high-rise buildings with roof overhangs, meaning that low-rise buildings in exposed locations can receive more wind-driven rain than high-rise buildings. The frontal vortex that forms upwind of high-rise buildings tends to prevent wind-driven rain from impinging on the middle and lower portions of the windward wall but results in concentrations of wetting at the upper edge and corners of the windward wall. Roof overhangs reduce wind-driven rain loads at these critical locations.

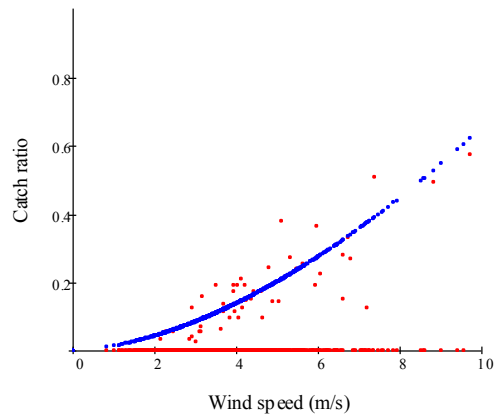
Local topography has a significant influence on wind-driven rain in the region, though east and south-east facing walls typically have the highest exposure. The building at Keefer is an exception within the study group, with wind during rain predominantly from the north-east. Buildings with high wind-driven rain intensities on north and north-

east facing walls may be more sensitive to corresponding high moisture loads because of the reduced benefit of solar-induced drying on those exposures. Significant variation between airport conditions and recorded building site data were also observed (Ge & Krpan, 2009), suggesting that designing buildings in Metro Vancouver based on site-specific data may be more appropriate than using airport data.

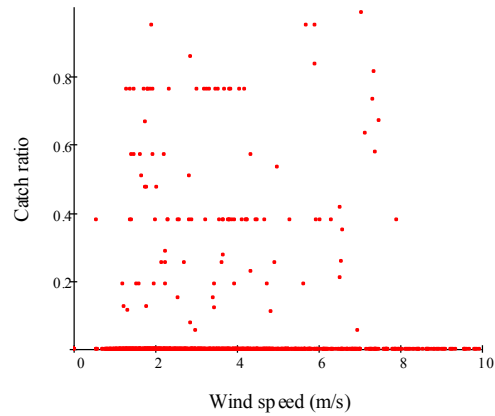
Overall, the wind-driven rain catch ratio measured in Metro-Vancouver is light compared to other climate regions, likely because of the characteristically low wind speeds and frequent instances of light to moderate rainfall intensity in the region. While maximum wind speeds tend to occur during dry hours, the average wind speed is higher during rain hours than during all hours. Persistent wind during rain combined with low rainfall intensity (and correspondingly small rain drop diameters), results in wind-driven rain loads of a unique nature producing long periods of wetness on building surfaces over the winter season.

#### 4.2 Analysis of historical airport data

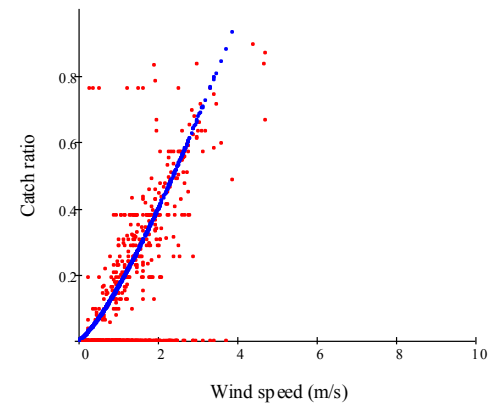
Following the approach of Choi (1998), the steps to establish water penetration test parameters include preparation of a database of historical hourly mean data for 25 or more years of record, including rainfall intensity and wind speed, and the corresponding peak wind speeds. The database of hourly and gust data is then transformed to a database of 5-minute mean rainfall intensities and 5-minute mean wind speeds. For each year, the highest 5-minute mean rainfall intensity and the highest 5-minute mean wind speed are then chosen. An extreme distribution analysis leads to a linear relationship between the return period and 5-minute mean rainfall intensity, wind speed, and calculated wind-driven rain intensity. These results are applied in the next section to compute water spray



***Kefer***



***Kingsway***



***Wallace***

Figure 36: Scatter plot of catch ratio as a function of wind speed showing curves fit to measured data for each building site

rate and air pressure differential. This section begins with a description of the data set and preprocessing steps and continues with an extreme distribution analysis of wind speed, horizontal rainfall intensity, and wind-driven rain intensity. The results for Wallace, the low-rise building without roof overhang, and Keefer, the high-rise building with overhang, demonstrate the significant influence of roof overhang on reducing wind-driven rain loads and show that high-rise buildings do not necessarily have higher loads.

#### *4.2.1 Description of data set and preprocessing steps*

A database of 25 years of measured rainfall intensity, wind speed, and gust speed is assembled from data obtained from Environment Canada for the Vancouver International Airport (YVR). The measured wind speed and direction are average hourly values and were collected from January 1st, 1981 to December 31st, 2005. The data set consists of 219144 one-hour periods (corresponding to 219143 indices numbered from zero). For periods with no measurement recorded, the measurement is taken as zero. The units for rainfall accumulation over each one hour period are given as tenths of a millimetre (i.e. the number of tenths of a millimetre that accumulate over each one hour period). These values are converted to rainfall intensity in millimetres per hour (mm/h) by multiplying the recorded value by 0.1. The wind speeds are recorded in kilometres per hour (km/h) and converted to metres per second (m/s) by dividing the recorded value by a conversion factor of 3.6.

#### *4.2.2 Wind speed*

For considerations of testing for rainwater penetration at the small cracks and openings within and around windows, a 5-minute averaging period is used to establish the mean wind speed (Choi, 1998; Sahal & Lacasse, 2008). For many meteorological

stations, including YVR, only hourly mean wind data and gust data is available. In these cases, the 5-minute mean data can be approximated from hourly data using Equation (2.22) proposed by Choi (1998) and rearranged as follows:

$$U_{5min} = (U_{gust} - U_{hrly}) \cdot \left[ \frac{\ln\left(\frac{300}{3600}\right)}{\ln\left(\frac{3}{3600}\right)} \right] + U_{hrly} \quad (4-2)$$

where

$U_{5min}$  = the mean wind speed with an averaging period of t seconds,

$U_{gust}$  = the gust speed based on an averaging period of 3 seconds, and

$U_{hrly}$  = the hourly mean speed.

For each of the 25 years of record at YVR, the maximum 5-minute mean wind speed so determined is selected to establish the extreme distribution of wind speeds, as shown below. The distribution is fitted by linear regression to establish the relationship between wind speed and return period, as shown in Figure 37. Based on this relationship, the maximum wind speed recorded at Wallace corresponds to 15-year return period.

#### 4.2.3 Horizontal rainfall intensity

The 5-minute rainfall intensity is obtained from the average hourly value using Equation (2.23), also proposed by Choi (1998), and rearranged as follows:

$$R_{h-5min} = \left[ \frac{60}{5} \right]^{0.42} \cdot R_{h-60min} \quad (4-3)$$

where

$R_{h-5min}$  is the horizontal rainfall intensity based on a 5 minute averaging period and

$R_{h-60min}$  is the horizontal rainfall intensity based on an hourly averaging period.

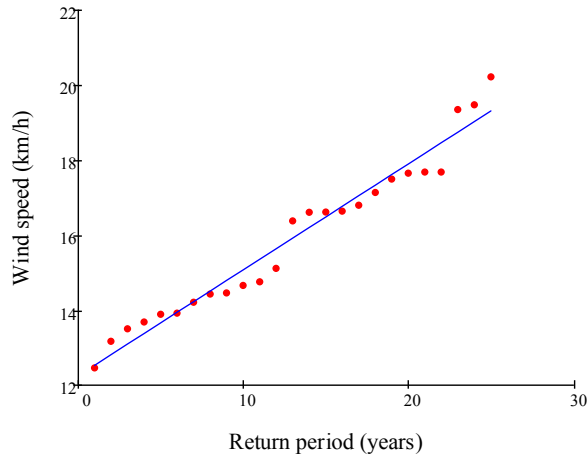


*Figure 37: Extreme distribution of wind speeds at the Vancouver airport*

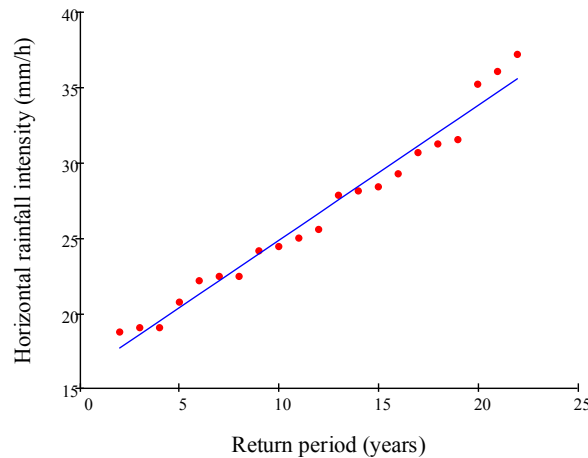


*Figure 38: Extreme distribution of horizontal rainfall intensity at the Vancouver airport*

Except for several outlying data points, the results show a linear correlation between horizontal rainfall intensity and return period, as shown in Figure 38. The extreme horizontal rainfall at the airport exceeds the maximum measured values at all three building sites for every year of record at the airport. The wind-driven rain intensity is calculated in the next section using the horizontal rainfall intensity and wind speed

measured at the airport and the expression for the governing case of catch ratio determined from the three building sites.

#### 4.2.4 *Wind-driven rain intensity*

The 5-minute mean wind-driven rain intensity is given by the product of the 5-minute mean horizontal rainfall intensity and the catch ratio, which is a function of corresponding 5-minute mean wind speed:

$$R_{wdr-5min} = R_{h-5min} \cdot \eta \quad (4-4)$$
$$\eta = f(U_{5-min})$$

The catch ratio is a function of wind-speed and is computed based on the results of Section 4.1.4. Both the horizontal rainfall intensity and the wind speed are measured at the airport and correspond to a specific return period. The wind speed at the airport is adjusted to the height of the building for this calculation, as described further in Section 4.3.1.

For each of the 25 years of record at YVR, the maximum 5-minute mean wind-driven rain intensity so determined is selected to establish the extreme distribution, as shown below in Figure 39. The outlying data is discarded and the distribution is fitted by linear regression to establish the relationship between wind-driven rain intensity and return period.

### 4.3 Calculation of test conditions and comparison to published values

To determine conditions for laboratory testing and noting that the provision for water-tightness is a serviceability requirement, the air pressure differential and water spray rate are often computed based on a 10-year return period. For this study, the test conditions for both 10- and 20-year return periods are computed.



#### 4.3.1 Air pressure differential

The air pressure differential is computed as follows based on the mean 5-minute wind speed corresponding to a 10-year return:

$$\text{Test pressure} = C_p \cdot \frac{1}{2} \rho \cdot U_{5min \text{ during rain-10y}}^2 \quad (4-5)$$

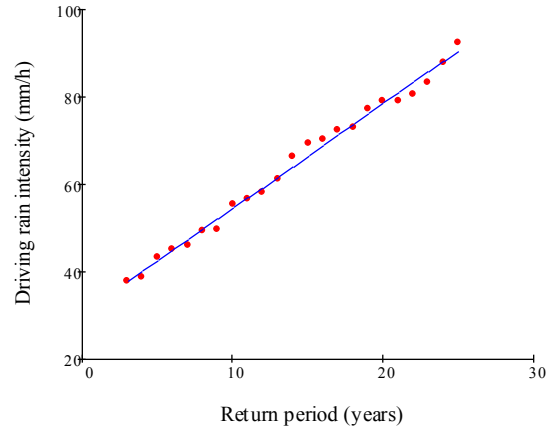


Figure 39: Extreme distribution of driving rain intensity

where

$C_p$  is the pressure coefficient,

$\rho$  is the air density taken as  $1.20 \text{ kg/m}^3$ , and

$U_{5min \text{ during rain-10y}}$  is the 5-minute mean wind speed during rain corresponding to a 10-year return period at the height of the building.

The pressure coefficient is taken as 1 to represent the critical value (Choi E. C., 1998).

This value is assumed to represent the combined interior and exterior pressure coefficients and therefore approximates the air pressure differential. The 5-minute mean wind speed is adjusted from 10 metres, which is the height of measurement at the airport, to the height of the building as follows:

$$U_Z = U_{10m} \cdot \left[ \frac{Z}{10} \right]^\alpha \quad (4.1)$$

where

$U_Z$  is the wind speed at height  $Z$ ,

$U_{10m}$  is the wind speed measured at height 10 m,

$Z$  is the height of the building, and

$\alpha$  is a coefficient to account for terrain roughness upwind of the building taken as 0.14 at the airport.

The results of the analysis are summarized in Table 10 and Figure 40 below and are compared to ASTM E331, and in the case of test pressure, to CSA A440, as well as a report on a study by Levelton (2006). The CSA A440 test pressure is the driving rain wind pressure (DRWP) at the Vancouver airport corresponding to a 10-year return period. Although the test pressure reported by Levelton is also based on the airport location, the results are not directly comparable to the current study. The Levelton study is based on 10 years of data from 12 stations where hourly rainfall rates, wind speeds and direction were measured. An extreme distribution was not computed. The DRWP is calculated for hours when rainfall exceeds 1.8 mm/h.

*Table 10: Estimated test pressures based on current study and summary of published values*

Source	Test pressure (Pa)
Current study (1/10 return)	202
Current study (1/20 return)	285
CSA A440 (1/10 return)	220
Levelton	162
ASTM E331	137

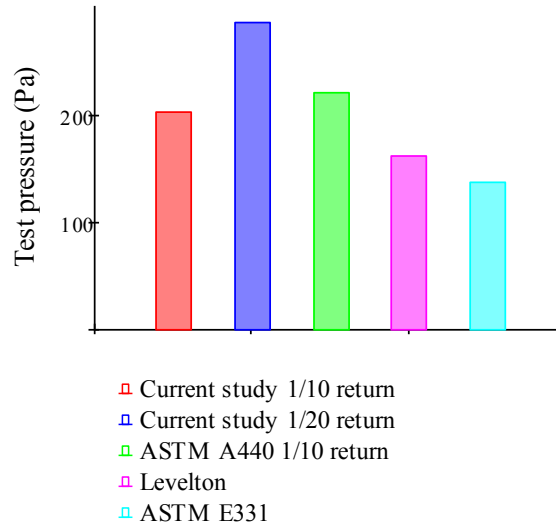


Figure 40: Bar chart showing estimated test pressures based on current study alongside published values

The estimated test pressure calculated for a 10-year return period is less than the CSA A440 standard test pressure of 220 Pa. The 285 Pa test pressure estimated for a 20-year return period exceeds the A440 standard. The estimated pressures for both return periods exceed the ASTM E331 standard test pressure of 137 Pa.

#### 4.3.2 Water spray rate

The water spray rate is taken equal to the driving rain intensity (mm/h) computed based on the historical airport data:

$$\text{Test spray rate} = R_{wdr-5min-10y} \quad (4-6)$$

where  $R_{wdr-5min-10y}$  is the 5-minute mean wind-driven rain intensity corresponding to a 10-year return period, as described in Section 0. The resulting water spray rates associated with 10- and 20-year return periods are summarized in Table 11 along with the test pressure specified in ASTM E331.

*Table 11: Estimated water spray rates associated with 10- and 20-year return periods and standard test spray rates*

Source	Water spray rate (mm/h)
Current study (1/10 return)	57
Current study (1/20 return)	80
ASTM E331	203

The estimated water spray rate is significantly less than the water spray rate specified in ASTM E331.

Overall, the results suggests that water spray rates specified for window tests are not representative of actual rainfall intensities likely to occur on real buildings, at least not in Metro Vancouver’s climate.

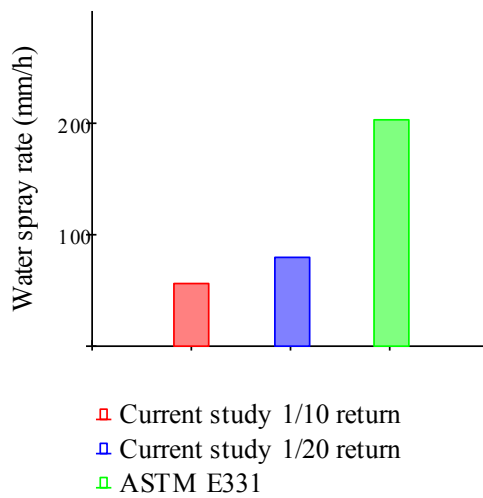


*Figure 41: Bar chart showing estimated water spray rates based on current study alongside published values*

## CHAPTER 5: CONCLUSIONS

### 5.1 Conclusions

Wind-driven rain is significantly influenced by building geometry, particularly roof overhang. Low-rise buildings may have higher catch ratios than high-rise buildings, meaning that low-rise buildings in exposed locations can receive more wind-driven rain than high-rise buildings. Local topography has a significant influence on wind-driven rain in the region, though east and south-east facing walls typically have the highest exposure. The wind-driven rain catch ratio measured in Metro-Vancouver is small compared to other climate regions, likely because of the characteristically light wind and frequent instances of light to moderate rainfall intensity in the region.

The estimated test pressure calculated for a 10-year return period is less than the CSA A440 standard test pressure of 220 Pa and seems to be adequate to simulate wind pressures in Metro Vancouver's climate based on the study sample. The estimated water spray rate is also less than the standard—ASTM E331—and appears to be adequate to simulate expected wind-driven rain over short periods of time. While the water spray rate estimated is significantly less than required by the standard, however, the test protocol as a whole may not realistically simulate actual moisture loads on window assemblies. The frequent instances of low intensity rainfall observed in this study may produce long durations of wetness that could pose risks to water penetration not simulated by the current tests. The results for Keefer, which has a large roof overhang on its eastern and most exposed side, reinforce findings from the literature that roof overhangs are a significant benefit in reducing wind-driven rain loads on buildings.

This thesis has led to the development of an analytical method to link field measurements to historical airport data to establish return periods. The results confirm anecdotal information on wetting patterns and the influence of building geometry that can help inform an engineering approach to building envelope design.

## 5.2 Future research

Collecting data for wind-driven rain research is one of the significant challenges facing researchers in this field. The gauges are costly to deploy and maintain, and many desirable locations for monitoring wind-driven rain are unsuitable for plate gauges. Because of their cumbersome appearance, many building owners would prefer not to have them on their buildings. Piezoelectric sensors are currently being used to measure horizontal rainfall intensity and may be adaptable to measuring wind-driven rain. Further research is required to explore this possibility.

While the existing test parameters for exterior moisture loads on buildings, including parameters for air pressure differential and water spray rate, may be adequate to test for short term exposure to high intensity wind-driven rain and provide a useful comparison for regulators, manufacturers and builders, these parameters may not adequately address duration of wetness common in Metro Vancouver's winter climate. Run-off may also significantly increase the moisture load at a particular location on the building. Further research is required to define realistic protocols to simulate duration of wetness and to improve designs to control water run-off. Effective run-off control strategies will not only reduce moisture loads and the associated risk of water ingress but may also help to optimize rain water harvesting techniques for buildings. Emerging techniques for modeling wind-driven rain using computational fluid dynamics (CFD)

combined with new and existing methods of taking measurements in the field may help to accelerate the advance of this work.

## REFERENCES

- Abernathy, F. (1968). Fundamentals of boundary layers. Massachusetts Institute of Technology, iFluids Program.
- American Architectural Manufacturers Association. (1994). *AAMA 501: Methods of test for exterior walls*. USA.
- American Society for Testing and Materials. (2000). *ASTM E331: Standard test method for water penetration of exterior windows, skylights, doors and curtain walls by uniform static air pressure difference*. USA.
- American Society for Testing and Materials. (2000). *ASTM E547: Standard test method for water penetration of exterior windows, skylights, doors and curtain walls by cyclic static air pressure difference*. USA.
- American Society of Heating, Refrigerating, and Air-Conditioning Engineers, Inc. (2009). Chapter 24: Airflow around buildings. In A. Handbook, *Fundamentals*. Atlanta.
- Australian and New Zealand Standards Institution. (1995). *AS/NZS 4284 Testing of building facades*.
- Barry, R. G. (1992). *Mountain weather and climate* (2nd ed.). London: Routledge, a division of Routledge, Chapman and Hall Inc.
- Beckett, H. E. (1938). *Building Research Note, No. 755*. UK: Building Research Station.
- Best, A. C. (1950). The size distribution of raindrops. *Quart. J. Royal Meteor. Soc.*, 76, 16 - 36.
- Birkeland, O. (1963). *Rain penetration investigations. A summary of the findings of CIB Working Commission on Rain Penetration*. Oslo: Norwegian Building Research Institute, Rapport 36.
- Blocken, B. (2004, May). Wind-driven rain on buildings: Measurements, numerical modeling and applications, Ph.D. Thesis. Belgium: Katholieke Universiteit Leuven.
- Blocken, B., & Carmeliet, J. (2004). A review of wind-driven rain research in building science. *Journal of Wind Engineering and Industrial Aerodynamics*, 92, 1079 - 1130.
- Blocken, B., & Carmeliet, J. (2004). On the validity of the cosine projection in wind-driven-rain calculations on buildings. Unpublished paper submitted to Building and Environment.
- Blocken, B., & Carmeliet, J. (2005). Guidelines for wind, rain and wind-driven rain measurements at test-building sites. *Symposium of Building Physics in the Nordic Countries*. Reykjavik.
- Blocken, B., & Carmeliet, J. (2005). High-resolution wind-driven rain measurements on a low-rise building--experimental data for model development and model validation. *Journal of Wind Engineering and Industrial Aerodynamics*, 93, 905 - 928.
- Blocken, B., & Carmeliet, J. (2005). On the accuracy of wind-driven rain measurements on buildings. *Building and Environment*.
- Blocken, B., & Carmeliet, J. (2005, July 28). Rain. *Building Physics Summer Course, Part III: Boundary conditions, Day three*. Montreal, Quebec, Canada: Concordia University.



- Blocken, B., Hens, H., & Carmeliet, J. (2002). Methods for the quantification of driving rain on buildings. *American Society of Heating, Refrigerating and Air-Conditioning Engineers Annual Meeting*, (pp. 338 - 350). Honolulu.
- Boyd, D. W. (1963). *Driving rain map of Canada, Technical Note No. 398*. Division of Building Research. Ottawa: National Research Council.
- British Standards Institution. (1992). *BS8104, Code of practice for assessing exposure of walls to wind-driven rain*. British Standards Institution.
- British Standards Institution. (2000). *BS EN 12155: Curtain walling water-tightness laboratory test under static pressure*.
- Canadian Standards Association. (2000). *CSA Standard A440.1 Windows user selection guide to CSA Standard A440-00, Windows*. Canada.
- Centre for Window and Cladding Technology. (1996). *CWCT Standard and good practice for curtain walling--Standard test method for water-tightness using static pressure*. UK.
- Chand, I., & Bhargava, P. K. (2001, December). Development of a rain gauge for measurement of directional distribution of wind driven rain on a horizontal plane. *Architectural Science Review*, 44(4), 391 - 394.
- Choi, E. C. (1994). Characteristics of the co-occurrence of wind and rain and the driving-rain index. *Journal of Wind Engineering and Industrial Aerodynamics*, 53, 49 - 62.
- Choi, E. C. (1994). Parameters affecting the intensity of wind-driven rain on the front face of a building. *Journal of Wind Engineering and Industrial Aerodynamics*, 53, 49 - 62.
- Choi, E. C. (1998). Criteria for water penetration testing. In R. J. Kudder, & J. L. Erdly (Eds.), *STP 1314, Water leakage through building facades*. West Conshohocken, PA: American Society for Testing Materials.
- Choi, E. C. (2001). Wind-driven rain and driving rain coefficient during thunderstorms and non-thunderstorms. *J. Wind Eng. Ind. Aerodyn.*, 89, 293-308.
- Chown, G. A., Brown, W. C., & Poirier, G. F. (1997). Evolution of wall design for controlling rain penetration. *Construction technology update*(No. 9). Ottawa: National Research Council, Institute of Research in Construction.
- Cornick, S., Dalglish, A., Said, N., Djebbar, R., Tariku, F., & Kumaran, M. K. (2002). *Report from Task 4 of MEWS project: Task 4 - Environmental conditions final report*. Institute for Research in Construction. Ottawa: National Research Council.
- Couper, R. R. (1974). Factors affecting the production of surface runoff from wind-driven rain. *2nd International CIB/RILEm Symposium on Moisture Problems in Buildings*. Rotterdam, the Netherlands.
- Day, J. A. (1966). *The science of weather*. Reading, Massachusetts: Addison-Wesley Publishing Company.
- Dingle, A. N., & Lee, Y. (1972, August). Terminal fallspeeds of raindrops. *Journal of Applied Meteorology*, 11, 877 - 879.
- Duchon, C. E. (n.d.). Observations of 1-minute rain rates using a vibrating-wire weighing-bucket rain gauge. Unpublished paper.
- Environment Canada. (1977). Chapter 19: Rate of fall - Tipping bucket rain gauge. In *MANOBS, Manual of surface weather observations*. Environment Canada, Meteorological Service of Canada.

- Environment Canada. (1977). Chapter 4: Atmospheric pressure. In *MANOBS, Manual of surface weather observations*. Environment Canada, Meteorological Service of Canada.
- Environment Canada. (1997). Chapter 3: Atmospheric phenomena. In *MANOBS, Manual of surface weather observations*. Environment Canada, Meteorological Service of Canada.
- European Committee for Standardization. (1997, October). Hydrothermal performance of buildings - Climatic data - Part 3: Calculation of a driving rain index for vertical surfaces from hourly wind and rain data. *Draft European Standard prEN 13013-3*.
- Fazio, P., Mallidi, S. R., & Zhu, D. (1995). A quantitative study for the measurement of driving rain exposure in the Montreal region. *Building and Environment*, 30(1), 1 - 11.
- Ge, H., & Krpan, R. (2007). Field measurement of wind-driven rain on a low-rise building in the coastal climate of British Columbia. *11th Canadian Conference on Building Science and Technology*. Banff.
- Ge, H., & Krpan, R. (2009). *Wind-driven rain study in the coastal climate of British Columbia, Final report*. British Columbia Institute of Technology, Building Science Centre of Excellence. Burnaby: Canada Mortgage and Housing Corporation, Home Owner Protection Office, British Columbia Housing Management Commission.
- Ge, H., Krpan, R., & Fazio, P. (2009). Field measurements of wind-driven rain: A study of seven buildings in Metro Vancouver. *12th Canadian Conference on Building Science and Technology* (pp. 37-48). Montreal: National Building Envelope Council.
- Hanington, I. (2006, July 16). City proposal offers community gardeners room to grow. *Westender*. Retrieved July 16, 2006, from <http://www.westender.com>
- Heidorn, K. C. (2001, May 1). *Air masses: A base for weather analysis*. Retrieved 10 15, 2011, from Weather phenomenon and elements: <http://www.islandnet.com/~see/weather/elements/airmasses.htm>
- Heidorn, K. C. (2004). *The BC weather book: From the Sunshine Coast to Storm Mountain*. Calgary: Fifth House Ltd., A Fitzhenry & Whiteside Company.
- Heidorn, K. C. (2005). *And now...The weather*. Calgary: Fifth House Ltd., A Fitzhenry & Whiteside Company.
- Hidore, J. J., & Oliver, J. E. (1993). *Climatology: An atmospheric science*. New York: Macmillan Publishing Company.
- Hogberg, A. B., Kragh, M. K., & van Mook, F. J. (1999). A comparison of driving rain measurements with different gauges. *5th Symposium on Building Physics in the Nordic Countries*. Gothenburg.
- Holmgren, J. (1946). Klimaets innflytelse pa materialer og byggemate. *Husbygging*, 1, 119-128.
- Huchon, N. B., & Handegord, G. O. (1989). *Building science for a cold climate*. Fredericton, New Brunswick: Construction Technology Centre Atlantic Inc. (Originally published by the National Research Council Canada).
- Inculet, D., & Surry, D. (1995). *Simulation of wind-driven rain and wetting patterns on buildings*. Canada Mortgage and Housing Corporation.

- International Organization for Standardization. (2005). *ISO/CD 15927-3 Hygrothermal performance of buildings - Calculation and presentation of climatic data -- Part 3: Calculation of a driving rain index for vertical surfaces from hourly wind and rain data - Committee draft*. International Organization for Standardization.
- Lacasse, M. A., Moore, T., & Van Den Bossche, N. (n.d.). *Water infiltration through openings in a vertical plane under static and dynamic pressure conditions (Slide presentation)*. Ottawa: Institute for Research in Construction, National Research Council Canada.
- Lacy, R. (1962). *An index of exposure to driving rain*. Garston: Building Research Station, Digest No. 23.
- Lacy, R. (1965). *Driving-rain maps and the onslaught of rain on buildings*. Building Research Station. Garston, England: Department of Scientific and Industrial Research.
- Lacy, R. E. (1951). Observations with a directional raingauge. *Q. J. Roy. Meteor. Soc.*, 77(332), 283-292.
- Lacy, R., & Shellard, H. (1962). An index of driving rain. *Meteorological Magazine*, 91, 177-184.
- Lee, J. (2005a). Boundary layer handout. *MECH 610: Fundamentals of fluid dynamics*. Montreal: McGill University.
- Levelton Engineering. (2006). *Wind-rain relationships in Southwestern British Columbia*. Ottawa: Canada Mortgage and Housing Corporation.
- Lutgens, F. K., & Tarbuck, E. J. (1989). *The atmosphere: An introduction to meteorology* (4th ed.). Englewood Cliffs, New Jersey: Prentice-Hall Inc.
- Massey, B. S. (1979). *Mechanics of fluids* (4th ed.). New York: Van Nostrand Reinhold Company.
- Maunder, W. J. (1968). Synoptic weather patterns in the Pacific Northwest. *Northwest Science*, 42, 80-88.
- McDonald, J. E. (1954). The shape of raindrops. In *Readings from Scientific America: The physics of everyday phenomena* (pp. 23-27). San Francisco: W. H. Freeman and Company.
- Nortest Standard. (1993). *NT BUILD 421 Roofs: Watertightness under pulsating air pressure*.
- Oke, T., & Hay, J. (1998). *The climate of Vancouver* (2nd ed., Vol. 50). University of British Columbia, Department of Geography.
- Panton, R. (1996). *Incompressible flow*. New York: John Wiley & Sons.
- Persson, A. (1998, July). How do we understand the Coriolis force? *Bulletin of the American Meteorological Society*, 79(7), 1374-1385.
- RDH Building Engineering. (2002). *Water penetration resistance of windows: Study of codes, standards, testing, and certification*. Ottawa: Canada Mortgage and Housing Corporation.
- Robinson, G., & Baker, M. C. (1975). *Wind-driven rain and buildings, Technical paper No. 445*. Ottawa: Division of Building Research, National Research Council of Canada.
- Sahal, N., & Lacasse, M. A. (2008). Proposed method for calculating water penetration test parameters of wall assemblies as applied to Istanbul, Turkey. *Building and Environment*, 43, 1250 - 1260.

- Singapore Standard. (1996). *SS 381: Materials and performance tests for aluminium curtain walls*. Singapore.
- Straube, J., & Burnett, E. (1997). Driving rain and masonry veneer. *ASTM Symp. Water Leakage Through Building Facades* (pp. 73-87). Orlando: American Society for Testing and Materials.
- Straube, J., & Burnett, E. (2000). Simplified prediction of driving rain on buildings. *International Building Physics Conference*. Eindhoven, the Netherlands.
- Straube, J., & Burnett, E. (2005). *Building science for building enclosures*. Building Science Press.
- Straube, J., & Burnett, E. (2005). Chapter 12: Rainwater control. In J. Straube, & E. Burnett, *Building science for building enclosures*. Building Science Press Inc.
- Straube, J., & Schumacher, C. (2006). *Driving rain loads for Canadian building design*. Waterloo, Ontario: Draft Report for Canada Mortgage and Housing Corporation.
- Tennekes, H., & Lumley, J. (1972). *A first course in turbulence*. Cambridge, Massachusetts: The MIT Press.
- van Mook, F. J. (1999). Full-scale measurements and numeric simulations of driving rain on a building. *10th International Conference on Wind Engineering*, (pp. 1145 - 1152). Copenhagen, Denmark.
- van Mook, F. J. (2002). *1.3 Literature survey*. Retrieved 12 10, 2003, from Driving rain on building envelopes:  
<http://sts.bwk.tue.nl/drivingrain/fjrvanmook2002/node5.htm>
- van Mook, F., de Wit, M., & Wisse, J. (1997). Computer simulation of driving rain on building envelopes. *2nd European and African Conference on Wind Engineering*. Genova.
- White, F. M. (2008). *Fluid mechanics* (6th ed.). McGraw Hill.
- World Meteorological Organization. (2008). *Guide to meteorological instruments and methods of observation, WMO-No. 8* (7th ed.). Geneva, Switzerland: World Meteorological Organization.
- Zhu, D., Mallidi, S. R., & Fazio, P. (1995). Approach for urban driving rain index by using climatological data recorded at suburban meteorological station. *Building and Environment*, 30(2), 229 - 236.
- Zhu, D., Mallidi, S. R., & Fazio, P. (1995). Quantitative driving rain exposure on a vertical wall at various Canadian cities. *Building and Environment*, 30(4), 533 - 544.

APPENDIX: BUILDING DETAILS AND SENSOR LOCATIONS

Keifer



Figure A7.1: Satellite image (left) of Building 7 and its surroundings of low-rise buildings, and photograph (right) showing the 12-storey high-rise residential building with a 3-foot overhang at roof level

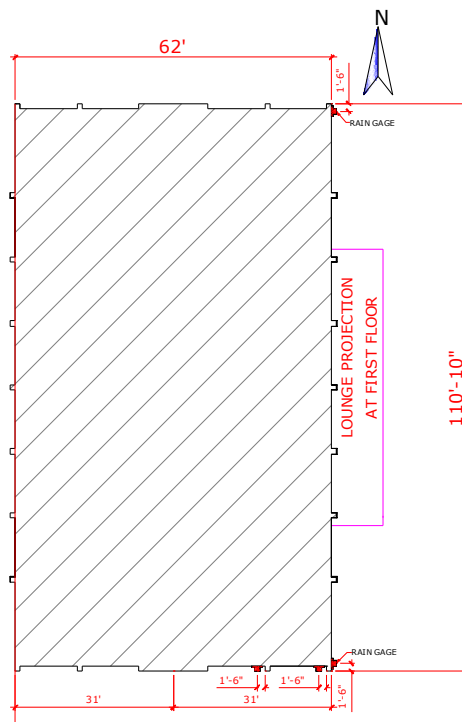
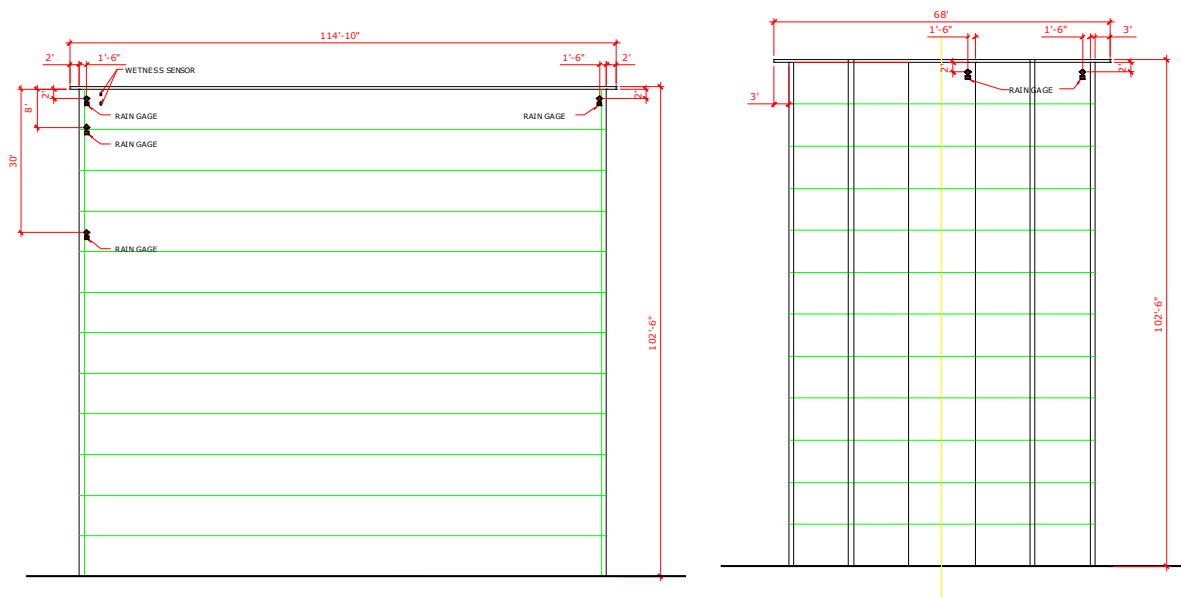


Figure A7.2: Plan view of Building 7



*Figure A7.3: Sketches of Building 7 showing the east elevation (left) with 4 gauges and the south elevation with 2 gauges*

## Kingsway



Figure A6.1: Satellite image (left) showing Building 6, which is surrounded by several high-rise buildings to the west and northeast and relatively few obstructions to south, and photograph (right) showing the east exposure of this 16-storey residential building clad with brick veneer and cast-in-place concrete

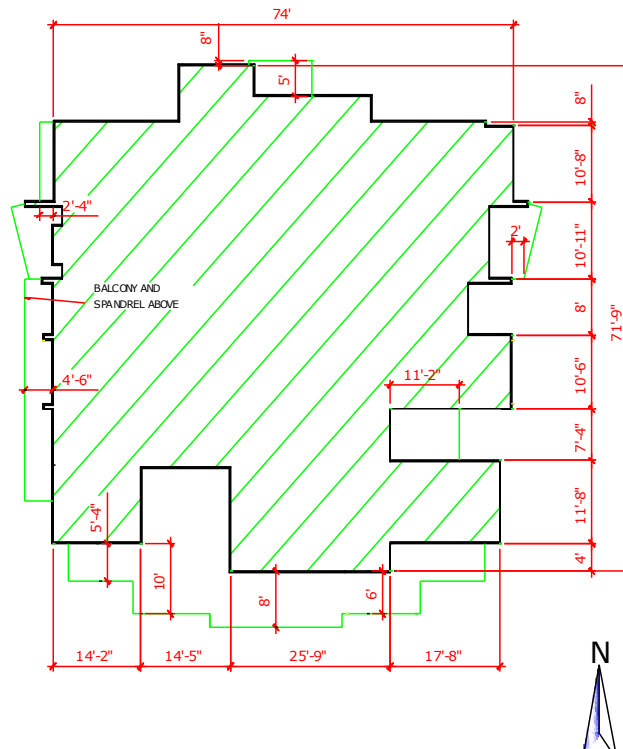


Figure A6.2: Plan view of Building 6

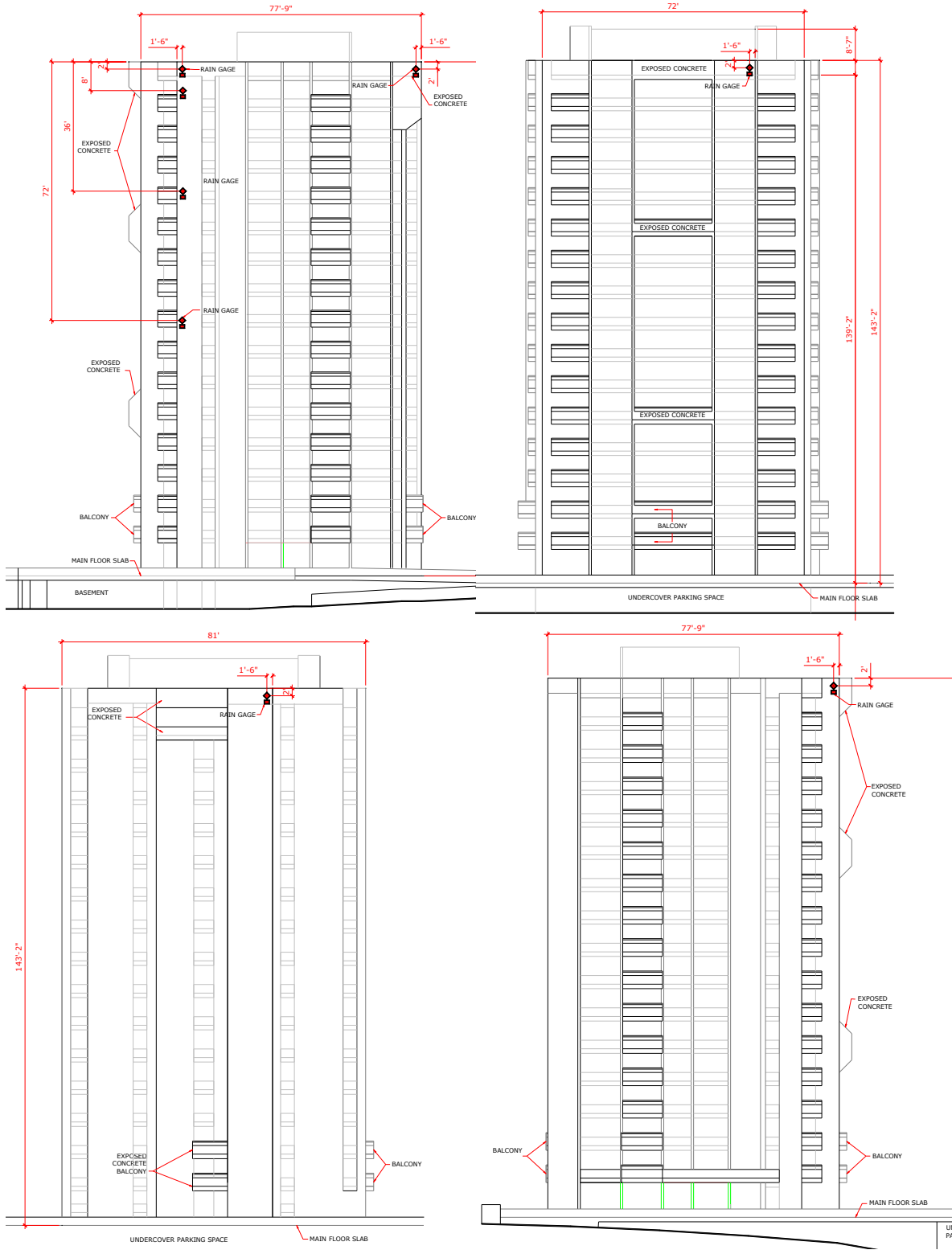


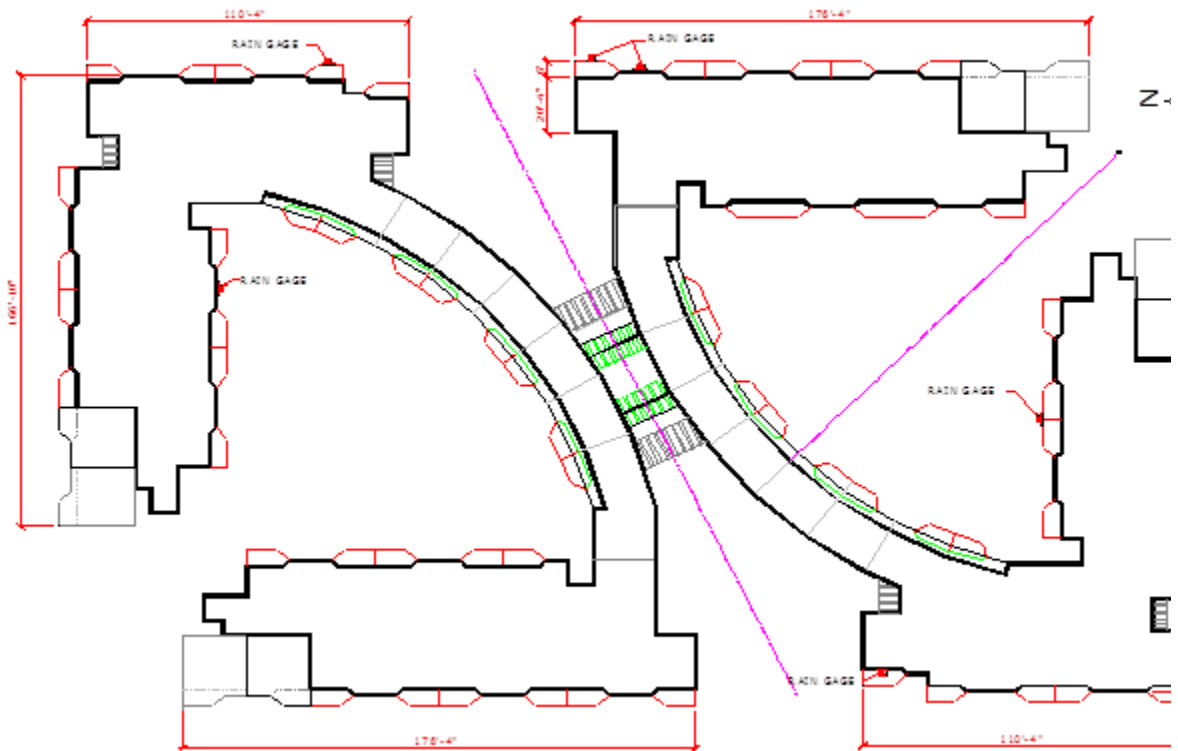
Figure A6.3: Sketches showing (clockwise from top left) the east elevation with 5 gauges, the south elevation with 1 gauge, the north elevation with 1 gauge, and the west elevation with 1 gauge



## Wallace



Figure A2.1: Satellite image (left) showing Building 2 and its surroundings including a parking lot to the north and parks to the south and west, photograph (right) showing the northern exposure, and site plan



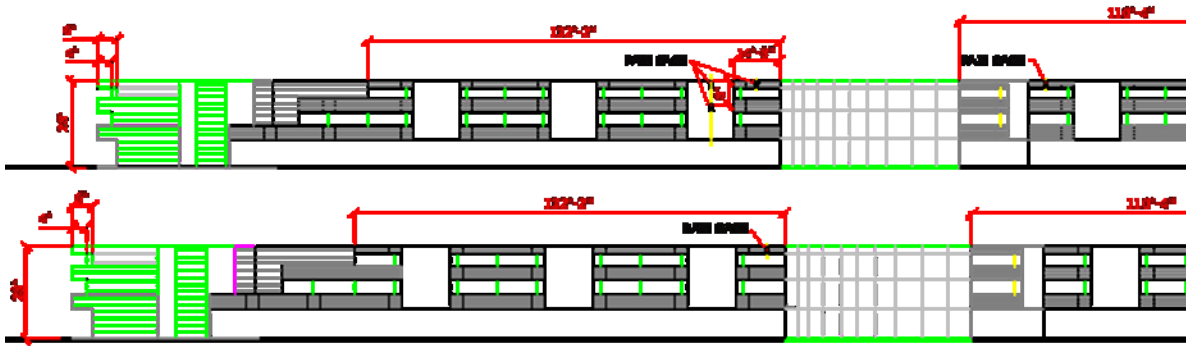


Figure A2.2: Sketches showing locations of rain gauges on Building 2: Plan view (top) with one gauge on the north wall and one gauge in the courtyard with a northern exposure, east elevation (middle) with three gauges, and west elevation (bottom) with one gauge